Comparing placentas from normal and abnormal pregnancies

Alex Heazell[*]   Simon Cotter   Laura Gallimore
David Greenhalgh   Stuart Kennedy   Vaclav Klika
Maurício Kritz   Poul Nielsen   Katharine Preedy   Ida Pu
Ani Setchi   Jennifer Siggers   Robert Whittaker[†]

Mathematics-in-Medicine Study Group
University of Strathclyde
September 2010

Abstract

This report describes work carried out at a Mathematics-in-Medicine Study Group. It is believed that placenta shape villous network characteristics are strongly linked to the placenta's efficiency, and hence to pregnancy outcome. We were asked to consider mathematical ways to describe the shape and other characteristics of a placenta, as well as forming mathematical models for placenta development.

In this report we propose a number of possible measure of placental shape, form, and efficiency, which can be computed from images already obtained. We also consider various models for the early development of placentas and the growth of the villous tree.

---

[*]Problem presenter.
[†]Report editor.

Contents

Part I
Introduction

1 Background

A healthy placenta is essential for a healthy outcome of pregnancy. At term, the human placenta is described as a discoid organ approximately 20–25 cm in diameter and 3 cm thick. The umbilical cord usually inserts in the centre of the placenta. The human placenta consists of a villous tree which is bathed in maternal blood. The villous tree contains fetal vessels, carrying fetal blood into terminal villi where it is brought into close proximity with maternal blood to optimise the transfer of nutrients and oxygen from mother to fetus and waste products in the opposite direction. As a result the function of the human placenta is very closely related to its structure.

A number of macroscopic and microscopic differences have been noted between normal placentas and those from intra-uterine growth restriction (where a baby does not meet its growth potential) and pre-eclampsia (where the mother develops high blood pressure and loses protein in her urine). These include macroscopic changes including: the shape of the placenta and the site of umbilical cord insertion (Biswas & Ghosh, 2008). Indeed, the combination of placental shape and cord insertion is hypothesised to affect the placental efficiency (Salafia & Yampolsky, 2009; Yampolsky *et al.*, 2009).

Data has been collected on placentas from women with normal pregnancies and from pregnancies complicated by reduced fetal movements (RFM). Women with RFM are at increased risk of stillbirth and intra-uterine growth restriction (Heazell & Frøen, 2008), so represent a group with a high possibility of abnormal placental structure (Warrander & Heazell, 2010). Preliminary data show that women with RFM have lighter, smaller placentas than women with normal pregnancies. Images of the fetal and maternal surfaces of the placenta have been taken, and can be used to examine the placental shape and the branching patterns of fetal blood vessels on the surface of the placenta.

The link between placental shape and poor pregnancy outcome is uncertain. What is certain is that placental shape is determined by events in early pregnancy. Immediately after implantation the embryo is spherical and is fully embedded in maternal tissue (decidua). Initially the placenta is formed from primary villi which undergo a series of branches. Over the early weeks of pregnancy, these villi branch and cells invade from the villi to convert the maternal uterine arteries that supply the developing fetus. The placental villi become vascularised with vessels growing from placental villi and towards blood vessels growing out from the base of the umbilical cord. When maternal blood supply starts, the placenta regresses from a sphere to a disc, if the maternal blood supply is abnormal this regression is uneven and irregular which will result in an abnormal placental shape and a non-central cord. Modelling the growth of the placental shape and the branching network of fetal vessels, may allow understanding of the factors that drive the development of placental shape, which cannot be viewed in real-time in human placental development.

2   Description of the placenta and its development

The human placenta consists of a villous tree which is bathed in maternal blood. The villous tree contains fetal vessels, carrying fetal blood into terminal villi where it is brought into close proximity with maternal blood to optimise the transfer of nutrients and oxygen from mother to fetus and waste products in the opposite direction. The function of the human placenta is very closely related to its structure.

The placenta is primarily a trade site for exchange of nutrients between maternal and fetal blood. It "provides anchorage, establishes a fetal vascular network in association with maternal blood supply but without connection" as well as hormonal support (Stewart, 2009). It acts as an endocrine gland with many physiological functions, such as immune protection. It has a large surface area which increases as the fetus grows.

The outer surface of the uterus is a glandular tissue called the epithelium. The endometrial stroma lies beneath this and is the tissue lining the uterus. Together, the glandular lining and the endometrial stroma are referred to as the endometrium of the uterus.

The development of the placenta includes the following phases: The blastocyte implants the uterine wall on the 6–7th day of gestation. This is followed by a pre-attachment phase, then an attachment phase. In the latter the blastocyte attaches to the epithelium, the outer lining of the uterus.

Then the epithelium is penetrated. Next follows an invasive phase when the endometrial stroma is penetrated. Then a reaction of the stromal cells follows. This is particularly marked in primates and rodents. The next thing that happens is interstitial implantation in which the blastocyte lies within the substance of the endometrium.

The histiotrophic phase is next. Histiotroph is an extracellular material derived from the endometrium and the uterine gland that accumulates in the space between the maternal and fetal tissues. This mechanism transfers nutrients from the mother to her fetus. This histiotrophic stage is short in humans. The haemotrophic phase follows. Haemotrophic nutrition is the exchange of blood-borne nutrients between the maternal and fetal circulations (Burton *et al.*, 2002).

Uterine glands provide histiopathic nutrition for the human fetus during the first trimester of pregnancy (Stewart, 2009). The developing embryo initially receives nutrients from milk-like secretions of the uterine tube. In the histiopathic phase it receives nutrition from the breakdown of tissues such as glands and stroma around the site of implantation. In the haemotrophic phase the embryo, and later fetus, receives nutrition from blood.

Figure 1 identifies some of the key stages in the development of the fetus. At time $t = 0$ the sperm reaches the egg and fertilises it. Within a couple of days the embryo leaves the Fallopian tube, reaches the uterus and embeds itself into the decidua of the uterine wall, where it receives nutrients from the maternal spiral arteries. There, it starts differentiating into a spherical structure. The placenta begins to develop upon implantation on one side of the sphere.

There are several hypotheses about how the villous tree develops based on the fact that it is hard to differentiate between different villi before they have been vascularised. One hypothesis is that villi grow one at a time with the extra one added only when the embryo becomes big enough to reach the next spiral artery. Another hypothesis is that initially there are 40–60 'roots' that develop simultaneously using the nutrient from the neighbouring spiral arteries but in the end the growing pattern is such that all villi are opposite a spiral artery. The first hypothesis is generally better accepted due to the fact that the width of a healthy placenta is relatively uniform and the size of each villa is very similar, meaning the villi tend to grow sideways rather than in all directions.

By time $t = 2$ weeks, one or two villi have developed on the surface to form a placenta of diameter 1 cm. By time $t = 4$ weeks it is possible to count between 5 and 10 villi in a surface of diameter approximately 2 cm. At this time the embryo begins to send blockers into the spiral arteries nearby

FIGURE 1: *Key stages in the development of an embryo. Photographs by Lennart Nilsson.*

FIGURE 2: *An embryo, vascularised blood vessels and a villous tree. Photograph by Lennart Nilsson.*

(*a*)   (*b*)
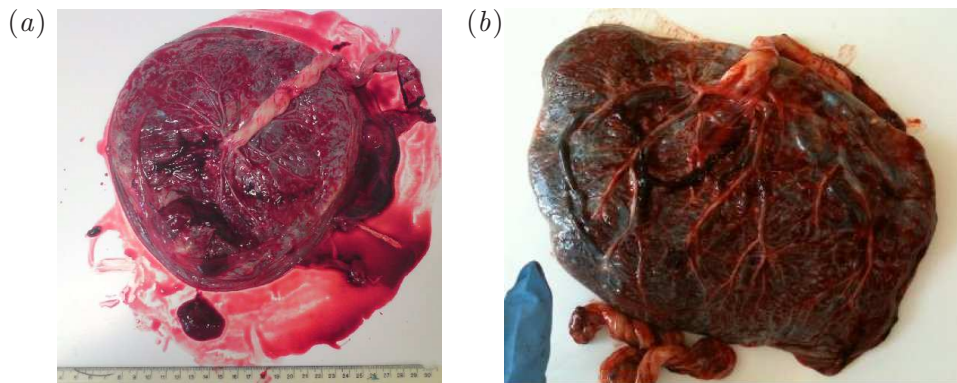
Figure 3: *Photographs of placentas: (a) A normal healthy placenta, and (b) a placenta with a lateral cord insertion point.*

and to reduce the nutrients being delivered by the maternal blood. It is believed that the villi continue to grow due to nutrients such as fats and sugars present in the uterine wall or the nutrients delivered by the spiral arteries away from the villi.

Until time $t = 7$ or $t = 8$ weeks the embryo is not physically connected to the villi. Around that time the umbilical cord that grows from the embryo reaches the placenta. The details surrounding this process are not known. One hypothesis is that the umbilical cord attaches itself to the place where the embryo first embedded itself into the uterine wall; another is that there are some factors that tell the embryo where the nutritional centre of mass of the placenta is.

In any case, fetal blood starts to perfuse the placenta and by time $t = 10$ weeks the villous tree has developed the maximum number of villi, is fully vascularised, the maternal spiral arteries have opened up and are feeding nutrients for both the embryo and placenta to grow (figure 2). By time $t = 40$ weeks the size of the placenta is around $20 \times 20 \times 3\,\mathrm{cm}^3$ and all the villi are lined up to be opposite some spiral artery.

3   Study group aims and objectives

In this project workshop we were specifically interested in developing models of:

1. The branching network of blood vessels on the fetal surface of the placenta from early pregnancy to term (which represents normal placental
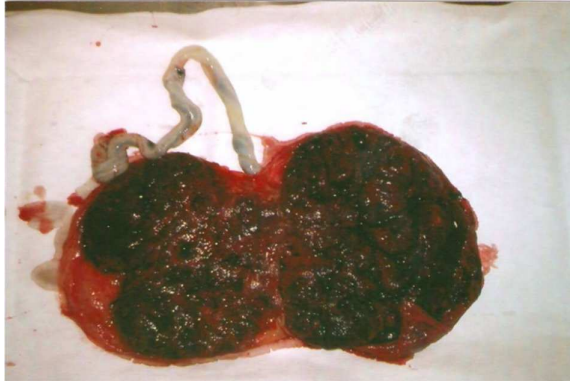
FIGURE 4: *A photograph of a bipartite placenta.*

structure).

2. By modelling the normal development of blood vessels, can inferences be made about the abnormal patterns seen in complicated pregnancies.

Using the expected models of placental development can valid measures be made to enable the comparison of:

1. The circularity of the placenta

2. The centrality of the umbilical cord insertion

3. The network of vessels on the fetal surface of the placenta

in normal and abnormal pregnancies.

To help with these tasks, various photographs of normal and abnormal placentas were available, along with some manual tracings of the the outline, cord insertion point and major fetal vessels. Some examples of these images are shown in figures 3 and 4, and the traces in figures 5 and 6.

Part II
Quantifying Placental Properties

We would like to clarify the link between placental shape and pregnancy outcome. In order to investigate this, we need to be able to objectively quantify key features of the placenta. Some of the key placental attributes highlighted by clinicians as being of interest include; size of the placenta, how centrally the umbilical cord is inserted and whether the placenta has a regular, circular shape.

The problem of correlating constitutive or functional behaviour of objects with their shape is not new. In 1966, Marc Kac published a paper entitled *Can one hear the shape of a drum?*, where he pointed out that concerns such as this goes back at least to the beginning of last century (Kac, 1966). The question posed by Mark Kac relates to comparing eigenvalues of the Laplacian operator with different domains (shapes) and have been answered in the negative by Gordon *et al.* (1992) for *non-convex* domains.

The 'functionality' of a drum is much simpler than that of placentas and the referred work shows that the problem is not easy. However, placentas are more convex than not. Moreover, we are considering placenta shapes from a visual stand and concerned also with the coverage of the baby's vascular network. Despite the differences, the analysis of the hearing problem provides hints about possible measures and measuring procedures.

There are many possibilities for quantifying placental shape. Yampolsky *et al.* (2008) describe measuring an average placental radius based on an equally spaced template having 20 sectors of 18°. The methods described here generalise their measures both with respect to where and to what to measure and take into account more of the available information.

4   Image data and processing

The available data for each placenta was the outline of the placenta, the site of the cord insertion and the position of the main fetal, placental arteries.
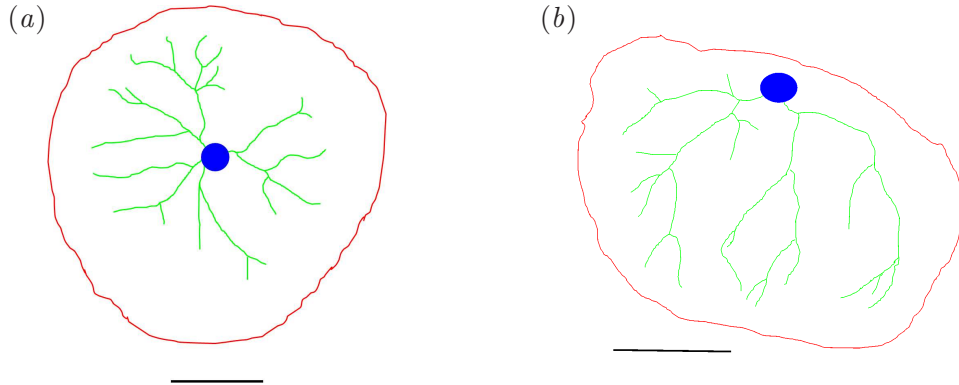
FIGURE 5: *Manually drawn traces of the two placentas in figure 3. The outline is shown in red, major vessels in green, the site of cord insertion in blue, and the scale bar in black. The placenta in (a) is normal, while that in (b) has a lateral cord insertion point.*

These outlines had been traced from photographs, manually in a computer drawing package. In order to distinguish easily the different structures, the placental outline was coloured red, the site of the cord insertion was coloured blue and the main arterial network was coloured green, whilst the scale bar was coloured black as shown in figure 5. The outline images were stored as tiff files.

The Matlab code to read in these images can be found in Appendix A. The files are read into Matlab as three-dimensional matrix. For example if the image is 200×300 pixels, Matlab reads this as a $200 \times 300 \times 4$ array, which can be thought of as four 200×300 pixel images stacked on top of each other. The first layer contains red values, the second green values and the third blue values, so these correspond to the placenta, vessel and cord outlines respectively. Each pixel has a number between 0 and 1, where 0 corresponds to the black background and 1 corresponds to the maximum intensity of that layer's colour. The fourth layer picks out all the outlines and the scale bar, so the scale bar can be isolated by subtracting off the other three images. In order to obtain binary images, the images are thresholded, so any pixel value below 0.5 is set to 0 and any pixel value above 0.5 is set to 1. The isolated features corresponding to the colour image in figure 5(a) are shown in figure 7.

From the number of pixels occupied by the scale bar, we are able to calculate the dimensions of each pixel in the images. We shall denote the width of each pixel by d_p.
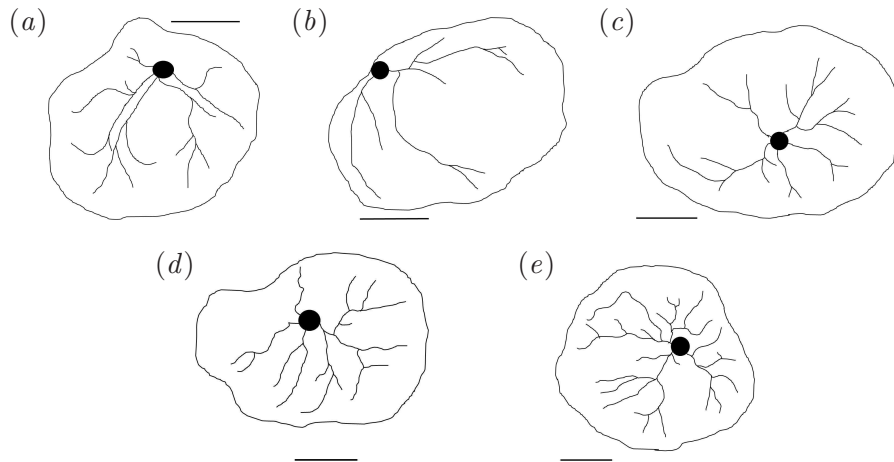
FIGURE 6: *Further traces of typical placentas shapes, showing the major vessels and cord insertion point. (a), (b) and (c) are RFM placentas, (d) and (e) are normal placentas. Observe that placentas (c) and (d) have a similar exterior shape, but quite different different vascular tree structures.*
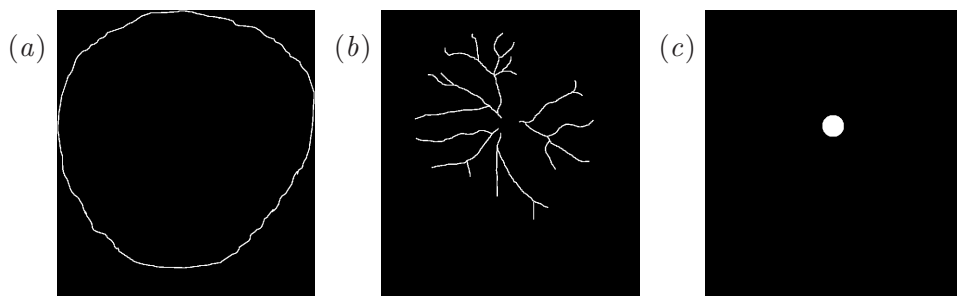
FIGURE 7: *Features extracted by Matlab from the colour image in figure 5(a): (a) the edge of the placenta, (b) the major vessels, and (c) the cord insertion point.*

For some of the calculations below, it will be necessary to determine which areas lie inside the placenta, and which lie outside. Matlab has an inbuilt command for filling shapes, allowing us to convert the outline of the placenta into a mask in which all the placenta pixels have the value 1 and all the background pixels have the value 0. We denote this mask matrix M_{ij}.

5 Placental shape and cord insertion point using moments

5.1 Cord insertion point

We would like quantify how central the site of cord insertion is, i.e. how far away the insertion point is from a 'central' point in the placenta. We define this central point as the centre of mass $\bar{\boldsymbol{x}}$ of the placenta, given by

$$\bar{\boldsymbol{x}} = \frac{1}{A} \iint \boldsymbol{x}\, \mathrm{d}A\,, \tag{5.1}$$

where

$$A = \iint \mathrm{d}A\,. \tag{5.2}$$

is the total area, and $\boldsymbol{x} = (x, y)$ is the position vector of each point inside the placenta.

These integrals over the placenta area can be approximated by summing over the pixels in the image, multiplying the mean value of the integrand in each square pixel by its area d_p^2. Since the mask M_{ij} takes the value 0 for pixels outside the placenta, and 1 for points inside, we can multiply by M_{ij} and then sum over all pixels to pick out the ones we require. It is convenient to introduce

$$N = \sum_{i,j} M_{ij}\,, \tag{5.3}$$

as the total number of pixels within the placenta area. The integrals for $\bar{\boldsymbol{x}}$ and A can then be approximated by

$$\bar{\boldsymbol{x}} \simeq \frac{1}{N} \sum_{i,j} M_{ij}\, (x_{ij}, y_{ij})\,, \tag{5.4}$$

$$A \simeq d_p^2 N \tag{5.5}$$

where (x_{ij}, y_{ij}) are coordinates of the centre of the (i, j)th pixel.

Since the cord is defined in the image by a region rather than a point, we use the same technique to calculate the centre of mass of the cord region, denoting this $\boldsymbol{x}_{\mathrm{cord}}$.

Having calculated A, $\bar{\boldsymbol{x}}$ and $\boldsymbol{x}_{\mathrm{cord}}$, we define our measure α of the centrality of the cord by

$$\alpha = \frac{|\boldsymbol{x}_{\mathrm{cord}} - \bar{\boldsymbol{x}}|}{\sqrt{A/\pi}}\,. \tag{5.6}$$

This is the distance between centres of the cord and the placenta, normalised by the radius of the circle with the same area as the placenta. This normalisation ensures that our measure of cord centrality is not affected by the size of the placenta. We note that $\alpha \geqslant 0$ and that α is zero if and only if the centre of the cord and the centre of the placenta coincide.

5.2   Circularity of placental shape

In order to consider measures of the shape of the placenta, we first introduce some notation,

$$\sigma_{xx}^2 = \frac{1}{A} \iint |x - \bar{x}|^2 \, \mathrm{d}A, \tag{5.7}$$

$$\sigma_{yy}^2 = \frac{1}{A} \iint |y - \bar{y}|^2 \, \mathrm{d}A. \tag{5.8}$$

Both σ_{xx}^2 and σ_{yy}^2 are variances which describe how spread out points in the placenta are from its centre of mass. We calculate the discrete approximations,

$$\sigma_{xx}^2 \simeq \frac{1}{N} \sum_{ij} M_{ij} \left(x_{ij}^2 - \bar{x}^2 \right), \tag{5.9}$$

$$\sigma_{xx}^2 \simeq \frac{1}{N} \sum_{ij} M_{ij} \left(y_{ij}^2 - \bar{y}^2 \right), \tag{5.10}$$

We define $\sigma^2 = \sigma_{xx}^2 + \sigma_{yy}^2$. We show in Appendix B that, for a given area, the shape which minimises σ^2 is a circle. The corresponding minimal value is found to be

$$\sigma_{\mathrm{circle}}^2 = \frac{1}{A} \iint x^2 + y^2 \, \mathrm{d}A = \frac{2\pi}{A} \int_0^{\sqrt{A/\pi}} r^3 \, \mathrm{d}r = \frac{A}{2\pi}. \tag{5.11}$$

In order to obtain a measure of how far the placenta is from circular, we consider how much σ^2 varies from $\sigma_{\mathrm{circle}}^2$. We define

$$\beta = \left(\frac{\sigma^2}{\sigma_{\mathrm{circle}}^2} - 1 \right)^{1/2} = \left(\frac{2\pi\sigma^2}{A} - 1 \right)^{1/2}. \tag{5.12}$$

This measure is constructed to have the property that it is zero for an exactly circular placenta and is positive otherwise. It depends only on the placenta shape (i.e. it is independent of the size). The square root is taken so that the

measure is linear in small deformations from a circle, and so better captures small deformations.

A similar calculation to (5.11), shows that for an ellipse with major axis length a and minor axis length b,

$$\sigma^2_{\text{ellipse}} = \frac{a^2 + b^2}{4}, \quad \Rightarrow \quad \beta = \left(\frac{a^2 + b^2}{2ab} - 1 \right)^{1/2}, \tag{5.13}$$

so if $a = 2b$, then $\beta = 1/2$.

5.3 Ellipticity of placental shape

Large β values, indicate poor circularity, but they fail to distinguish between two key classes of shape — the placenta could either be a regular oval shape, with a smooth edge, or a very irregular, possibly lobed shape without a direction in which it is elongated. We would therefore like to obtain one or more additional measures that describe how elliptical a given placenta shape is.

To do this, we consider the covariance matrix,

$$\mathbf{C} = \left(\begin{array}{cc} \sigma^2_{xx} & \sigma^2_{xy} \\ \sigma^2_{xy} & \sigma^2_{yy} \end{array} \right), \tag{5.14}$$

where σ^2_{xx} and σ^2_{yy} are as defined above, and

$$\sigma^2_{xy} = \frac{1}{A} \iint (x - \bar{x})(y - \bar{y}) \, \mathrm{d}A \simeq \frac{1}{N} \sum M_{ij}(x_i y_i - \bar{x}\bar{y}). \tag{5.15}$$

Since $\mathbf{C}$ is a real symmetric matrix, it has a complete set (two in this case) of orthogonal eigenvectors. The two eigenvectors define the two principal directions for the shape. The sizes of the eigenvectors give the degrees of elongation or compression in these two directions. If the placenta has an axis about which it is elongated, then the eigenvector corresponding to the larger of the the two eigenvalues, points along this axis. We select σ^2_a to be the larger of the two eigenvalues and σ^2_b the smaller. The ratio of the eigenvalues

$$\lambda = \frac{\sigma_a}{\sigma_b} \geq 1, \tag{5.16}$$

tells us how elongated the placenta is, with the minimal value of 1, corresponding to no elongation in any particular direction. (This could correspond to a circle or a more irregular shape with no preferred direction.)
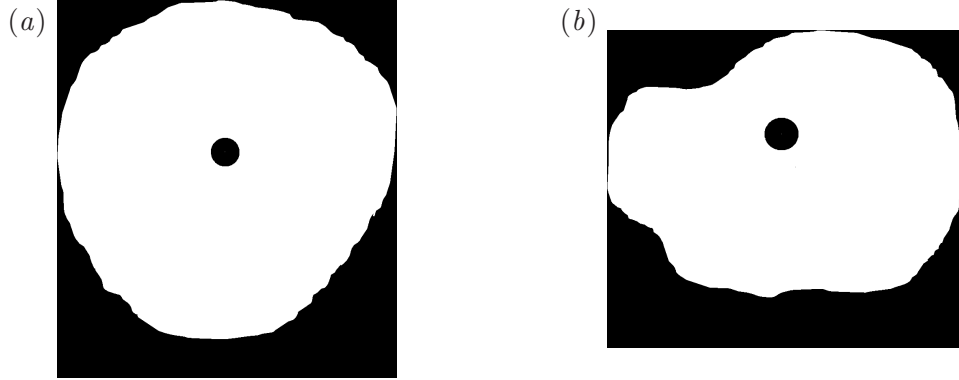
FIGURE 8: *Outlines of two example placentas, with the cord insertion points shown. (a) A reasonably circular placenta, with $\alpha = 0.0756$, $\beta = 0.0802$, $\gamma = 0.0724$ and $\lambda = 1.05$. (b) A more irregular and less circular placenta, which has $\alpha = 0.237$, $\beta = 0.268$, $\gamma = 0.136$ and $\lambda = 1.38$.*

Analogously to β, we would like to consider how much the placenta varies from the best-fitting ellipse. We define this ellipse to have the same area A and aspect ratio λ as the placenta. So if the ellipse has semi-axes a and b, we require

$$A = \pi a b, \qquad \frac{\sigma_a}{\sigma_b} = \frac{a}{b}, \qquad (5.17)$$

which implies

$$a = \left(\frac{A\sigma_a}{\pi\sigma_b}\right)^{1/2}, \qquad b = \left(\frac{A\sigma_b}{\pi\sigma_a}\right)^{1/2}. \qquad (5.18)$$

Substituting for a and b in Equation (5.13) we see

$$\sigma^2_{\text{ellipse}} = \frac{A}{4\pi}\left(\frac{\sigma_a^2 + \sigma_b^2}{\sigma_a\sigma_b}\right) = \frac{A\sigma^2}{4\pi\sigma_a\sigma_b}, \qquad (5.19)$$

(The second equality results from the fact that $\sigma^2 = \sigma_a^2 + \sigma_b^2$, as the sum of the eigenvalues of a matrix is equal to its trace.)

Our corresponding measure of departure from an ellipse is therefore given by

$$\gamma = \left(\frac{\sigma^2}{\sigma^2_{\text{ellipse}}} - 1\right)^{1/2} = \left(\frac{4\pi\sigma_a\sigma_b}{A} - 1\right)^{1/2}. \qquad (5.20)$$

That this measure does achieve its minimum value of zero, for an ellipse is shown in Appendix B.

Measure	Definition	Description
Cord Offset	$\alpha = \dfrac{\|\boldsymbol{x}_{\text{cord}} - \bar{\boldsymbol{x}}\|}{\sqrt{A/\pi}}$	Normalised offset of cord from centre. $\alpha = 0$ is central, larger α for larger deviations.
Circularity	$\beta = \left(\dfrac{2\pi\sigma^2}{A} - 1\right)^{1/2}$	Deviation from a circle. $\beta = 0$ for a perfect circle; larger β for larger deviations.
Ellipticity	$\gamma = \left(\dfrac{4\pi\sigma_a\sigma_b}{A} - 1\right)^{1/2}$	Deviation from an ellipse. $\gamma = 0$ for a perfect ellipse; larger γ for larger deviations.
Aspect Ratio	$\lambda = \dfrac{\sigma_a}{\sigma_b}$	Ratio of longer to shorter axis. $\lambda = 1$ for symmetry, larger λ for higher ratios.

TABLE 1: *A summary of the four measures proposed in §5.*

5.4   Summary of proposed measures

In this section, we have proposed four measures α, β, γ, and λ to quantify the centralness of of the cord insertion point and the shape of the placenta. A summary of these measures, is given in table 1, and two example placenta are shown in figure 8, along with the values of the measures.

It should be noted that β, γ, and λ are not independent, i.e. any one can be computed from the values of the other two. However, as we are unsure of the clinical significance of the different aspects of the placenta shape, it would be best to consider all three to begin with.

6   Placental shape from rule and compass

6.1   The shape-observation problem

We are interested not only in the geometry of the border of the placenta but also in the localization of the allantois with respect to this border. Furthermore, it would be nice to identify whatever allows for distinguishing normal pregnancy placentas from reduced fetal movement (RFM) placentas (see figure 6).

It is quite clear that we can momentarily disregard the thickness and the shell-like form of their 'superior' face, together with its curvature, and consider placentas as 2-dimensional geometric forms. Moreover, each placenta is a single piece whatever the pregnancy and its shape is connected.

Hence, let $\Omega \subset \mathbb{R}^2$ be a simply connected domain in the plane and $\partial\Omega$ its boundary. Denoting the closure of Ω by $\Omega^{\bullet}$ and its interior by Ω°, we have that:

$$\partial\Omega = \Omega^{\bullet} \setminus \Omega^{\circ}. \qquad (6.1)$$

The border $\partial\Omega$ of Ω is usually a 1-dimensional continuous variety (a line), not necessarily differentiable nor convex. It is, nevertheless, closed and without extremities dividing $\mathbb{R}^2$ into two disjoint regions.

6.2   Shape inspectors

To inspect the shape of Ω, or of $\partial\Omega$, let us consider measurement templates formed by a finite collection of points: one interior to Ω, $\mathbf{P} \in \Omega^{\circ}$, and N other points $\mathbf{P}_i \in \mathbb{R}^2 \setminus \Omega^{\bullet}$, $\forall i \in \{1, \ldots, N\}$, exterior to it. Without loss of generality, the exterior points can be taken on a circle encompassing Ω (see figure 9). Based on these templates, some geometrical constructs and measures will be developed for inspecting 2D-shapes. These templates are nevertheless not fixed. Both the points and the number of points may vary during an inspection procedure. Hence, the templates may be taken as parameters for the measures. The set of rays defined in equation (6.2) will be denoted by π^r and the set of lines defined in equation (6.3) by π^l. It is expected that the simple mathematical objects here described will contribute to establish data collection procedures to enlarge data about placentas consistently and coherently.

We have that $\mathbf{P} \notin \partial\Omega$ and $\mathbf{P}_i \notin \partial\Omega, \forall i = 1, \ldots, N$. Let

1. the rays starting at $\mathbf{P}$ and extending in the direction of $\mathbf{P}_i$ which are parametrically described as:

$$\overrightarrow{\mathbf{PP}_i}(\lambda) = \mathbf{P} + \lambda(\mathbf{P}_i - \mathbf{P}) = (1 - \lambda)\mathbf{P} + \lambda\mathbf{P}_i, \lambda \geq 0, \qquad (6.2)$$
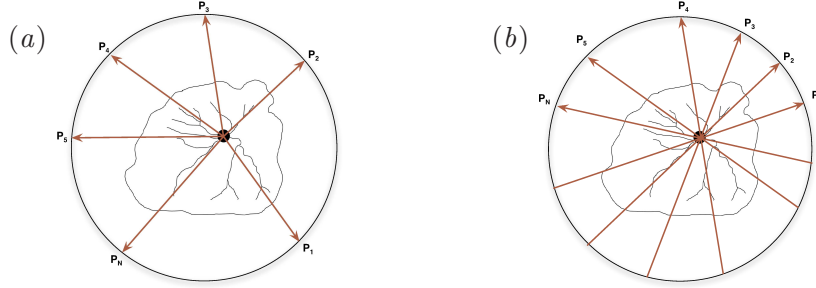
FIGURE 9: *Measuring Templates: (a) rays and (b) lines.*

2. and the lines passing through $\mathbf{P}$ and each $\mathbf{P}_i$ which are parametrically described as:

$$\overline{\mathbf{PP}_i}(\lambda) = \mathbf{P} + \lambda(\mathbf{P}_i - \mathbf{P}) = (1 - \lambda)\mathbf{P} + \lambda\mathbf{P}_i, \lambda \in \mathbb{R}. \qquad (6.3)$$

Then $\mathbf{PP}_i(0) = \mathbf{P}$ and $\mathbf{PP}_i(1) = \mathbf{P}_i, \forall i = 1, \ldots, N$. In the case of placenta shapes the point P will generally coincide with the allantois, as suggested in figure 9, but not necessarily.

Furthermore, since $\partial\Omega$ is closed and $\mathbf{P}$ and $\mathbf{P}_i$ are 'inside' and 'outside' $\partial\Omega$, respectively, the rays $\overrightarrow{\mathbf{PP}_i}(\lambda)$ intersect $\partial\Omega$ at least in one point and the lines $\overline{\mathbf{PP}_i}(\lambda)$ at least in two points. Let

$$\partial_r\Omega_i = \partial\Omega \cap \{\overrightarrow{\mathbf{PP}_i}(\lambda), \lambda > 0\} \qquad (6.4)$$

and

$$\partial_l\Omega_i = \partial\Omega \cap \{\overline{\mathbf{PP}_i}(\lambda), \lambda \in \mathbb{R}\}. \qquad (6.5)$$

If $\#(A)$ denotes the cardinality of a set A, we have that:

Lemma 6.1. *If Ω is bounded, $\#(\partial_r\Omega_i)$ is odd and $\#(\partial_l\Omega_i)$ is even.*

Proof. Trivial. ($\mathbb{R}^2$ is a Haursdorf space and $\partial\Omega$ divides $\mathbb{R}^2$ in two non-intersecting regions) $\qquad\qquad\square$

By introducing the notation, $\partial_l^+\Omega_i = \partial\Omega \cap \{\overline{\mathbf{PP}_i}(\lambda) \mid \lambda > 0\}$ and $\partial_l^-\Omega_i = \partial\Omega \cap \{\overline{\mathbf{PP}_i}(\lambda) \mid \lambda < 0\}$, the set of intersection points between lines and $\partial\Omega$ can be described as:

$$\partial_l\Omega_i = \partial_l^+\Omega_i \cup \partial_l^-\Omega_i, \qquad (6.6)$$

where the sets $\partial_l^+\Omega_i$ and $\partial_l^-\Omega_i$ are analogous to $\partial_r\Omega_i$ and both $\#(\partial_l^+\Omega_i)$ and $\#(\partial_l^-\Omega_i)$ are odd.

Definition 6.1. *A set S is convex if and only if given a finite set $\{u_1, \ldots, u_p\}$ in S, all barycentric combinations of $\{u_1, \ldots, u_p\}$ also belong to S, that is,*

$$\sum_{i=1}^{p} \lambda_i u_i \in S, \tag{6.7}$$

where $0 \leq \lambda_i \leq 1, \forall 1 \leq i \leq p$ and

$$\sum_{i=1}^{p} \lambda_i = 1. \tag{6.8}$$

It is clear that one can consider $p = 2$ without loss of any sort, particularly when $S \subset \mathbb{R}^2$. (Usually p is chosen to be equal to the dimension of S to simplify convexity tests.) Convexity can be relaxed in many situations by considering star-shaped domains. More information about mathematical properties of convex domains and their algebra can be found in (Rockafellar, 1970, Parts I–III) and (Rockafellar & Wets, 1998, Chap. 2 and 3).

Definition 6.2 (Star-shapedness). *A set $S \subset \mathbb{R}^2$ is star-shaped if and only if there exists a point $\mathbf{c} \in S$ such that for any other point $\mathbf{P} \in S$ the segment $\overline{\mathbf{c}\mathbf{P}} \subset S$.*

We say that S is star-shaped with respect to the central point $\mathbf{c}$. The central point $\mathbf{c}$ is not unique in general. The set of all possible central points of a star-shaped domain S is a convex set and is called the convex-kernel of S Smith (1968). In the sequel, $B_\rho(P)$ will denote a ball of radius ρ centred at P.

Lemma 6.2. *Let Ω be bounded and $\partial_l \Omega_i$ be given by equation 6.5. If $\#(\partial_l \Omega_i) = 2$, for any $\mathbf{P} \in \Omega^\circ$ and $\mathbf{P}_0 \in \mathbb{R}^2 \setminus \Omega^\bullet$, then Ω is star-shaped if $\mathbf{P}$ is held fixed inside Ω and convex if the $\mathbf{P}$ varies throughout Ω°.*

Proof. Whenever $\#(\partial_l \Omega_i) = 2$, we have that $\partial_l \Omega_i = \{\mathbf{q}, \mathbf{Q}\}$. Let us first introduce some useful notation. Given a pair of points $\{\mathbf{q}, \mathbf{Q}\}$, we define

$$[\mathbf{q}, \mathbf{Q}] = \{\eta\mathbf{q} + (1 - \eta)\mathbf{Q}, \eta \in [0, 1]\} \tag{6.9}$$

and

$$(\mathbf{q}, \mathbf{Q}) = \{\eta\mathbf{q} + (1 - \eta)\mathbf{Q}, \eta \in (0, 1)\} \tag{6.10}$$

to be respectively the closed and open segments connecting the points $\mathbf{q}$ and $\mathbf{Q}$. Note that, for $\{\mathbf{q}, \mathbf{Q}\} = \partial_l \Omega_i$, $[\mathbf{q}, \mathbf{Q}] = \Omega^\bullet \cap \overline{\mathbf{P}\mathbf{P}_0}$ and $(\mathbf{q}, \mathbf{Q}) = \Omega^\circ \cap \overline{\mathbf{P}\mathbf{P}_0}$.

The proof proceeds as follows. Since Ω is bounded, there is a large enough ρ_0 such that $\Omega^\bullet \subset B_{\rho_0}(\mathbf{P})$. For any point $\mathbf{P}' \in \Omega^\circ, \mathbf{P}' \neq \mathbf{P}$, let $\mathbf{P}_0 = \partial B_{\rho_0}(\mathbf{P}) \cap \overrightarrow{\mathbf{P}\mathbf{P}'}$. We have that both $\mathbf{P}$ and $\mathbf{P}'$ belong to the segment $(\mathbf{q}, \mathbf{Q})$ and thus the segment $[\mathbf{P}, \mathbf{P}']$ belongs to Ω°. Therefore, Ω is star-shaped with respect to the central point $\mathbf{P}$.

Letting $\mathbf{P}$ vary inside Ω, the above reasoning shows that $[\mathbf{P}, \mathbf{P}'] \subset \Omega$ for all $\mathbf{P}, \mathbf{P}' \in \Omega$. Therefore, Ω is convex. $\qquad\square$

The placenta traces in figure 6 look like being either convex or star-shaped at the given resolution.

Towards *measuring* forms, let's begin considering the following values:

$$d_i^r = min_{\mathbf{q} \in \partial_r \Omega_i} d(\mathbf{P}, \mathbf{q}), \tag{6.11}$$

for the rays, and

$$\begin{aligned} d_i^l &= \min(\delta_i^-, \delta_i^+), \\ D_i^l &= \max(\delta_i^-, \delta_i^+), \end{aligned} \tag{6.12}$$

where

$$\delta_i^- = \min_{\mathbf{q} \in \partial_l^- \Omega_i} d(\mathbf{P}, \mathbf{q}), \tag{6.13}$$

$$\delta_i^+ = \min_{\mathbf{q} \in \partial_l^+ \Omega_i} d(\mathbf{P}, \mathbf{q}). \tag{6.14}$$

Note that if $\#(\partial_r \Omega_i) = 1$, then $d_i^r = d(\mathbf{P}, \mathbf{q})$, since $\partial_r \Omega_i = \{\mathbf{q}\}$. Likewise, if $\#(\partial_l \Omega_i) = 2$, then

$$\begin{aligned} \delta_i^- &= d(\mathbf{P}, \mathbf{q}^-), \\ \delta_i^+ &= d(\mathbf{P}, \mathbf{q}^+); \end{aligned} \tag{6.15}$$

where $\partial_l^- \Omega_i = \{\mathbf{q}^-\}$ and $\partial_l^+ \Omega_i = \{\mathbf{q}^+\}$.

The following measures associated with Ω and the templates π^r and π^l may be defined and are straightforward to evaluate:

$$E_1(\Omega, \pi^r) = \max_{k=1}^{N}(d_i^r) / \min_{k=1}^{N}(d_i^r), \tag{6.16}$$

$$E_2(\Omega, \pi^l) = \max_{k=1}^{N}(D_i^l / d_i^l), \tag{6.17}$$

$$E_2'(\Omega, \pi^l) = \min_{k=1}^{N}(d_i^l / D_i^l), \tag{6.18}$$

$$E_3(\Omega, \pi^l) = \max_{k=1}^{N}(D_i^l) / \min_{k=1}^{N}(d_i^l), \tag{6.19}$$
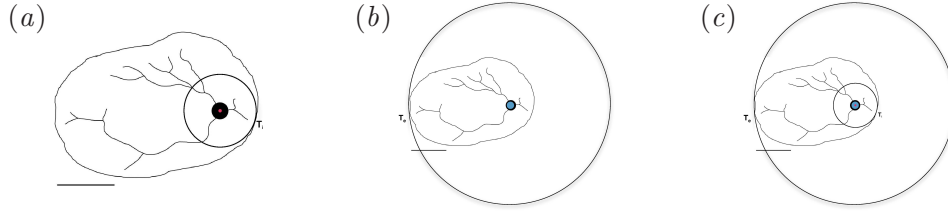
FIGURE 10: *Encircling a placenta from inside and outside: (a) from inside, (b) from outside and (c) both.*

$$E_3'(\Omega, \pi^l) = \min_{k=1}^{N}(D_i^l)/max_{k=1}^{N}(d_i^l), \tag{6.20}$$

$$E_4(\Omega, \pi^l) = \max_{k=1}^{N}(D_i^l + d_i^l)/\min_{k=1}^{N}(D_i^l + d_i^l). \tag{6.21}$$

To define the next measure, let

$$B_R(\mathbf{P}, \Omega) = \bigcap_{\rho>0} B_\rho(\mathbf{P}) \quad \text{such that} \quad \Omega \subset B_\rho(\mathbf{P}), \tag{6.22}$$

and

$$B_r(\mathbf{P}, \Omega) = \bigcup_{\rho>0} B_\rho(\mathbf{P}) \quad \text{such that} \quad B_\rho(\mathbf{P}) \subset \Omega. \tag{6.23}$$

That is, $B_R(\mathbf{P}, \Omega)$ is the *smallest* ball centred at $\mathbf{P}$ containing Ω and $B_r(\mathbf{P}, \Omega)$ is the *largest* ball centred at $\mathbf{P}$ and contained in Ω (see figure 10). Then,

$$E_5(\Omega, \mathbf{P}) = R/r. \tag{6.24}$$

The measure E_5 and the exterior and interior tangent points $\mathbf{T}_e$ and $\mathbf{T}_i$ are not as straightforward to obtain as the previous ones. The finding of $B_R(\mathbf{P})$ and $B_r(\mathbf{P})$ require a limiting process that must be approximated.

6.3   About placental shapes and measures

The following comments about placental shapes and the measures proposed above are intended as guidelines and navigation lights in gathering data and in the further exploration of any relationship between placental conformation and function. First, comments about the shape.

The shape of placentas has always been described by Dr. A. Heazell as a discoid; not a circle or an ellipsoid. If we consider that it must be covered without failure by the baby's vascular network and that the blood flow

should be the most efficient possible, we should preferably be considering star-shaped placentas rather than almost circular ones. If the baby's vessels had no dimension at all, a star-shaped placenta would permit that each of its points be reached by a straight vase, shortening the time the blood needs to flow back and forth.

Of course they are not dimensionless. The effective branching network allows for conforming a shortest path reach with the limited number of branches that may growth from any convergence point. The ability to branch at any point in any direction would require convexity (see Lemma 6.2). However, the finiteness of the branching could easily fill a star-shaped area. From another stand, the irregularities presented by placentas at their borders may conform to star-shaped constrains.

Moreover, we need to remind us that while operational the placenta does have a curvature and is not planar. We should take this into account while measuring and design correcting procedures for the measurements.

Second, we highlight some characteristics of the measures proposed.

- $E_1(\Omega, \pi^r)$ is a measure of circularity. The larger the number of external points $\mathbf{P}_i$ and the close the measure is to 1, the greater the chances that the domain be circular.
  However, star-shaped domains with regular variations at the border or with variations nearby the $\mathbf{P}_i$ may trap E_1-measurements into giving the impression of circularity.

- The measure $E_2(\Omega, \pi^l)$ indicates whether there is a radial symmetry around $\mathbf{P}$.

- For shapes in the form of ellipses, R is the longer axis while r is the shortest. Besides that, the lines $\overline{\mathbf{PT}_e}$ and $\overline{\mathbf{PT}_i}$ are collinear to the ellipse's axis. The measure E_5 and the exterior and interior tangent points $\mathbf{T}_e$ and $\mathbf{T}_i$ in figure 10 provide indications about eccentricity and aspect ratio if Ω is close to an ellipsoid.

A deeper investigation about these measures and their properties is needed and shall be addressed in future work.

7   Index of efficiency for the vascular network

7.1   Introduction

It is expensive and time consuming to obtain three-dimensional images of human placentas and, at present, not possible to do so in utero. However, photographs of the fetal side of the placenta yield a good approximation of the fetal arterial network and it is possible that scans may be able to obtain such images in utero. It has been observed that the size of the placenta and the topology of the fetal arterial network may be related to the outcome of the pregnancy. The mechanisms behind the relationship are unknown and it may well be that the size of the placenta is, at least in part, determined by the same factors which influence the arterial network. This index does not seek to disentangle mechanisms, rather, it provides a means of comparing placentas in a consistent and reproducible manner by defining the 'efficiency' with which they facilitate transfer of toxins and nutrients between the fetus and the mother.

7.2   Defining the index

We only have information about the fetal arterial network on the fetal surface of the placenta. We must, therefore, make some fairly heroic assumptions about the villous network which underlies it. The volume of the placenta consists of a villous network bathed in maternal blood so we assume that this network is uniformly distributed throughout the placenta and, similarly that the network of capillaries carrying maternal blood is matched to the fetal network. The narrow vessels that comprise the villous network offer significant resistance to blood flow, particularly compared to the wider vessels of the arterial network seen on the fetal surface of the placenta so we neglect the resistance in the surface arteries and restrict our attention to the villous network. We assume further that the contribution to transfer from each point of the placenta is inversely proportional to the distance it has to travel through the villous network (given a fixed rate of flowm, this could be considered in terms of units of nutrient/toxin per unit time). Ideally we'd like to calculate the distance to the set of lobules which from the entry to the surface arterial network. Unfortunately, however, at this point the photographs of placentas do not allow all tips to be located. (Typically there may be 10-20 tips in the photograph and it is known that placentas contain 40-60 lobules) We, therefore calculate the contribution of a given point to be inversely proportional to the distance from the nearest point on the arterial network. In addition, since the placenta is a 3 dimensional object and the

villi are situated below the surface network, we define the contribution from a point $\mathbf{x}$ on the 2 dimensional picture of the fetal arterial network to be

$$C_x \propto \frac{1}{d+1} \tag{7.1}$$

where d is the shortest distance from $\mathbf{x}$ to the fetal arterial network. Because we are looking for an index rather than absolute numbers we may define

$$K_x = \frac{1}{d+1} \tag{7.2}$$

Thus total 'efficiency', E, of the placenta is then determined by integrating K_x over the fetal surface of the placenta, Ω.

$$E = \int_\Omega \frac{1}{d+1} \tag{7.3}$$

7.3 Calculating E from photographs

There are numerous well understood algorithms for calculating the shortest distance from a surface to a finite number of points. However, the problem of the shortest distance to a network of lines is more complex. We describe a method below which gives a good approximation of the shortest distance. We start with picture which consists of the lines of the arterial network, the boundary of the placenta and and a scale bar 5 cm long. We render this as and RGB tiff file in which the centre of the placenta is red, the arterial network green and the scale bar blue. Reading this in to R (R Development Core Team, 2009) (or Matlab) gives 4 matrices R, G, B, and V of which we are interested in the first three which represent respectively the Red, Green and Blue values of each pixel within the tiff file. The R consists of zeros except in the interior of the placental boundary. Similarly, G consists of zeros except on the arterial network and B has positive numbers only on the scale bar.

- set t=number of nonzero entries in R.

- We start with a matrix M in which all entries are 0 except those on the arterial network which are set to 1 and define c=number of nonzero entries in G

- if entry $x = 1$ on M and its neighbour $y = 0$ corresponds to a non-zero entry on the R then set $y = 2$ and increment c by 1.

- whilst $c < t$, if entry $x = v$ on M and its neighbour $y = 0$ corresponds to a non-zero entry on the R then set $y = v + 1$ and increment c by 1.

- let $l=$ number of columns in B with a nonzero entry. The length represented by each pixel is $p = \frac{5}{l}$

- the distance of each pixel from the arterial network $D = p(M - 1) + 1$ and the area of each pixel is p^2

- Efficiency $E = p^2 \sum \frac{1}{D}$

See appendix C for R code which implements this algorithm.

7.4 Results

Figure 12 shows the input derived from placental photographs on the left and a picture of the distances to the nearest point on the arterial network together with the index of efficiency and the maximum distance between a point on the placenta and the nearest point on network on the right. It can be seen that in placentas of similar size, a well vascularised placenta will have a greater efficiency. However, a larger placenta (as in figure $12c$) will have a greater efficiency index than a smaller placenta.

An initial analysis of 53 placental traces suggests that pregnancies with reduced fetal movement have lower efficiencies than those from normal pregnancies (see figure 11). However, a protocol for producing traces needs to be developed and a more rigorous investigation carried out before we can place confidence in such results.

7.5 Discussion

The index defined above offers a means of comparing placentas with quite different sizes and arterial networks without requiring knowledge of parameters difficult or impossible to obtain. It relies on some fairly heroic assumptions, in particular that the maternal network is well matched to the arterial network and that the contribution from each point is inversely proportional to the distance to the nearest point on the arterial network. This last assumption is, at best, an approximation because we know that the villous network will join the arterial network at the tips. However, this index is calculated from traces drawn by eye on digitised photographs of full-term placentas. There is, inevitably, a good deal of noise associated with these pictures both in identifying all the core arteries and in tracing them to the tips. Figure $12(d)$ shows an example of a placenta in which the umbilical
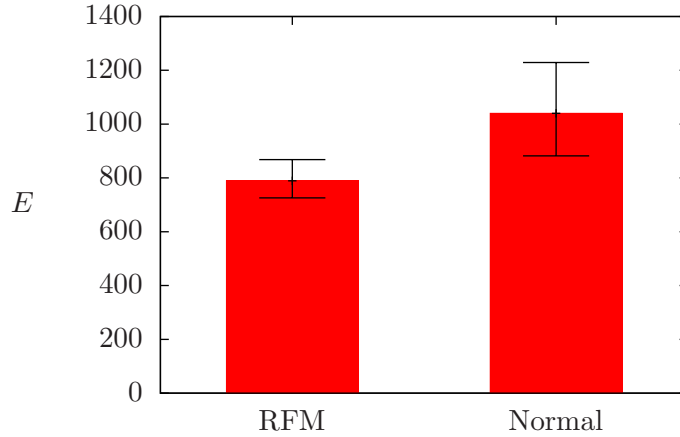
FIGURE 11: *Initial results for the efficiency index E for a set of placentas from 52 pregnancies, with 30 classified as having RFM and the remaining 23 normal.*

cord covers part of the surface and therefore what looks like an area with no vascularisation (on the right of the umbilical insertion) is, in fact, an area lacking information.

The algorithm, although it gives an approximation of distance, does not take into account increasing distance along the diagonals. However, this inaccuracy is small in comparison to the noise in the input traces. In addition, although the pixel size has been taken into account in calculating the index, the resolution varies between pictures. A protocol for photographing and tracing the network would go a long way to resolve these problems and it would be possible to revert to calculating the distance to the nearest tip. Even with the crude approximations described, we see a difference in the mean efficiencies of placentas associated with normal births and those associated with reduced fetal movement.

The next section derives a rigorous measure of blood transfer. However, it depends on parameters which may vary between placentas so a development which combined both approaches to achieve a better estimate of the relationship between distance to the arterial tips and contribution to efficiency in this approach and a protocol for photographing full term placentas would provide a robust means to compare full term placentas. If in utero images of the fetal surface of the placenta were to become available, the same method could be used to compare them.

(a)   efficiency= 1039.287   max dist= 4.566 $d = 4.566\,\mathrm{cm}$ $E = 1039.287$

(b)   efficiency= 848.575   max dist= 5.969 $d = 5.969\,\mathrm{cm}$ $E = 848.575$

(c)   efficiency= 1506.379   max dist= 3.953 $d = 3.953\,\mathrm{cm}$ $E = 1506.379$

(d)   efficiency= 913.162   max dist= 5.754 $d = 5.754\,\mathrm{cm}$ $E = 913.162$

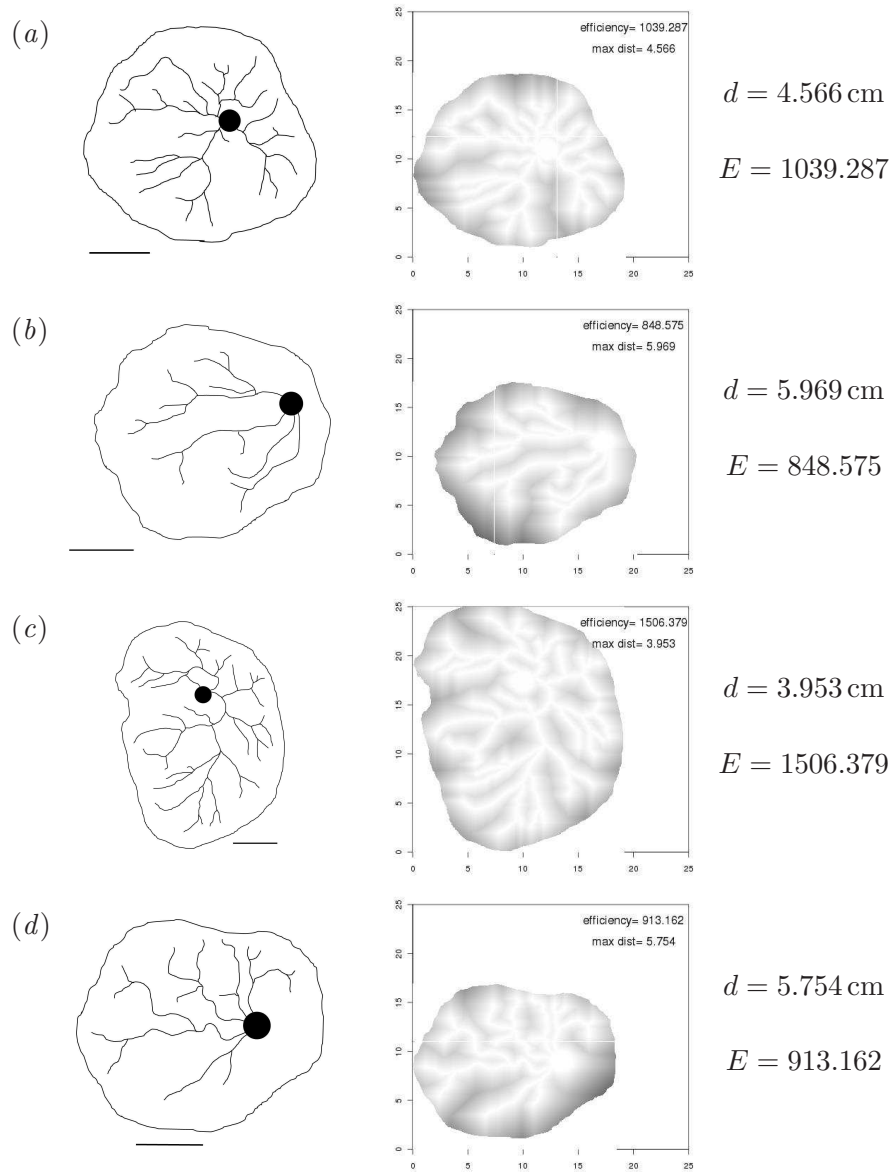FIGURE 12: *Diagrams of the fetal surface of a placenta. The left-hand column shows a trace of the visible fetal arterial network with a 5cm scale bar. The central column shows contour maps of the shortest distance to the arterial network. The right-hand columns gives the maximum shortest distance d and the efficiency index E. (a), (c) and (d) show placentas from normal pregnancies; (b) is from one with reduced fetal movement.*

Part III

Mathematical Modelling

8 Mechanical model to quantify the blood flow

8.1 Introduction

Assuming that the baby's blood is sufficiently well bathed in the mother's blood during transit, it will become fully oxygenated during its transit through the placenta. Thus the question of how efficient is a given placenta is how much flow can travel through the placenta for a given pressure drop between the arteries and the vein in the umbilical cord. The cord will only be able to tolerate a given pressure drop, and this places a maximum on the blood that can flow through the placenta. In this section we develop a network model of the vessels that are visible on the ultrasound image and use a porous medium model of the unseen vessels. For the large vessels we assume they are rigid and contain Poiseuille flow, and in the small vessels we neglect effects of compliance. With these assumptions the overall model is linear, meaning that the total flow through the placenta is proportional to the overall pressure drop between the arteries and the vein in the umbilical cord. Our aim in this section is to develop rules for finding the constant of proportionality.

8.2 Porous medium model of blood flow in the placenta

8.2.1 Model development and simplification

We assume that a two-dimensional image of the shape of a placenta and tracings of the major vessels are provided, and attempt to use this to predict the blood flow through the given placenta. We treat flow in the small arterial and venous vessels within the placenta as flow in two porous media, following work by Chernyavsky *et al.* (2010) in which a more detailed porous medium model of a single lobule was considered, and by Bonfiglio *et al.* (2010) in which a porous medium model of the blood flow in a liver

lobule was modelled. We assume that the terminal end points of the visible vessels act as point sources for the arterial flow and point sinks for the venous flow (thus the invisible vessels are treated as part of the porous medium). In this section we prescribe the fluxes, but in Section 8.3 we develop a model that can be solved to find them. We denote the flux out of the ith arterial vessel end by Q_{ai} and that into the ith venous vessel end by Q_{vi}.

The flows in the arterial and venous networks are governed by Darcy's equation:

$$\boldsymbol{u}_a = -\frac{k_a}{\mu}\boldsymbol{\nabla}p_a, \qquad \boldsymbol{u}_v = -\frac{k_v}{\mu}\boldsymbol{\nabla}p_v, \qquad (8.1)$$

where $\boldsymbol{u}_a$ is the spatially averaged arterial velocity, k_a is the arterial permeability and p_a is the pressure in the arterial vessels, and similarly for the venous vessels (but with subscript v) and μ is the blood viscosity. We also apply mass conservation for the arterial and venous vessels respectively:

$$\boldsymbol{\nabla}\cdot\boldsymbol{u}_a = -\lambda\left(p_a - p_v\right), \qquad \boldsymbol{\nabla}\cdot\boldsymbol{u}_v = \lambda\left(p_a - p_v\right), \qquad (8.2)$$

where λ is the volume flux of blood transferring from the arterial to the venous vessels per unit volume of tissue per unit pressure drop between the arterial and venous vessels. Note that positive divergence indicates creation of mass and negative divergence indicates loss of mass. The boundary conditions are no flux of blood through the outer boundary of the placenta, that is $\hat{\boldsymbol{n}}\cdot\boldsymbol{u}_a = \hat{\boldsymbol{n}}\cdot\boldsymbol{u}_v = 0$ at the boundary.

Introducing $p_1 = p_a - p_v$ and $p_2 = k_a p_a + k_v p_v$, we obtain

$$\nabla^2 p_1 - K^2 p_1 = 0, \qquad \nabla^2 p_2 = 0, \qquad (8.3)$$

where $K^2 = \mu\lambda(k_a^{-1} + k_v^{-1})$. Noting that p_1 and p_2 can only be singular at the point sources and sinks with at most a logarithmic singularity at these points, p_1 and p_2 must have the form

$$p_1 = \tilde{p}_1 + \sum_{\text{vessels } i} A_i\,\mathrm{K}_0(Kr_i), \qquad p_2 = \tilde{p}_2 + \sum_{\text{vessels } i} B_i\ln r_i, \qquad (8.4)$$

where r_i is the distance to the ith source/sink, A_i and B_i are constants, K_0 is a modified Bessel function of zeroth order and $\tilde{p}_1$ and $\tilde{p}_2$ are analytic functions. We enforce

$$\oint_{C_i} \hat{\boldsymbol{n}}_i\cdot\boldsymbol{u}_a\,\mathrm{d}l = \frac{Q_{ai}}{h}, \qquad \oint_{C_i} \hat{\boldsymbol{n}}_i\cdot\boldsymbol{u}_v\,\mathrm{d}l = -\frac{Q_{vi}}{h}, \qquad (8.5)$$

where h is the depth of the placenta (assumed constant) and C_i is a small circle around the end of the vessel, and obtain

$$\oint_{C_i} \hat{\boldsymbol{n}}_i \cdot \boldsymbol{\nabla} p_1 \, \mathrm{d}l = -\frac{\mu}{h} \left(\frac{Q_{ai}}{k_a} + \frac{Q_{vi}}{k_v} \right) , \qquad \oint_{C_i} \hat{\boldsymbol{n}}_i \cdot \boldsymbol{\nabla} p_2 \, \mathrm{d}l = \frac{\mu}{h} \left(Q_{vi} - Q_{ai} \right) .$$
$$(8.6)$$

In turn this means that, for all i,

$$A_i = \frac{\mu}{2\pi h} \left(\frac{Q_{ai}}{k_a} + \frac{Q_{vi}}{k_v} \right) , \qquad B_i = \frac{\mu}{2\pi h} \left(Q_{vi} - Q_{ai} \right) . \qquad (8.7)$$

Since during development the lobule grows as a whole, it is reasonable to assume that it is not possible to transfer from one lobule to another during one transit of the placenta. In turn this means that $Q_{ai} = Q_{vi} = Q_i$, and hence

$$A_i = \frac{K^2 Q_i}{2\pi h \lambda}, \qquad B_i = 0. \qquad (8.8)$$

The boundary conditions become $\hat{\boldsymbol{n}} \cdot \boldsymbol{\nabla} p_1 = \hat{\boldsymbol{n}} \cdot \boldsymbol{\nabla} p_2 = 0$ at the boundary, which implies that $\tilde{p}_2$ is constant, and we may take it to be zero by fixing the gauge pressure.

8.2.2   Statement of the simplified problem

The problem to be solved for $\tilde{p}_1$ reads

$$\nabla^2 \tilde{p}_1 - K^2 \tilde{p}_1 = 0 \qquad (8.9)$$

in the placenta, subject to

$$\hat{\boldsymbol{n}} \cdot \boldsymbol{\nabla} \tilde{p}_1 = -\frac{K^2}{2\pi h \lambda} \sum_{\text{vessels } i} Q_i \, \hat{\boldsymbol{n}} \cdot \boldsymbol{\nabla} \, \mathrm{K}_0(K r_i) \qquad (8.10)$$

$$= \frac{K^3}{2\pi h \lambda} \sum_{\text{vessels } i} Q_i \hat{\boldsymbol{n}} \cdot \hat{\boldsymbol{t}}_i \, \mathrm{K}_1(K r_i) \qquad (8.11)$$

on the boundary of the placenta, where $\boldsymbol{t}_i$ is the vector from the source/sink to the point of interest, $r_i = |\boldsymbol{t}_i|$ and $\hat{\boldsymbol{t}}_i = \boldsymbol{t}_i / r_i$. Note that $\mathrm{K}_0' = -\mathrm{K}_1$ and $\mathrm{I}_0' = \mathrm{I}_1$ (Abramowitz & Stegun, 1964, equation 9.6.27). Once $\tilde{p}_1$ is found we find

$$p_a = \frac{k_v}{k_a + k_v} p_1, \quad p_v = -\frac{k_a}{k_a + k_v} p_1, \quad \boldsymbol{u}_a = -\frac{\lambda}{K^2} \boldsymbol{\nabla} p_1, \quad \boldsymbol{u}_v = \frac{\lambda}{K^2} \boldsymbol{\nabla} p_1,$$
$$(8.12)$$

where

$$p_1 = \tilde{p}_1 + \frac{K^2}{2\pi h\lambda} \sum_{\text{vessels } i} Q_i \, \mathrm{K}_0(Kr_i). \tag{8.13}$$

Note that, since there are singularities in the pressure at the ends of the vessels, we can only estimate the pressure in the vessels by finding the pressure on a circle about the singularity whose radius equals the vessel radius.

8.2.3 Special case with exact solution

The simplest case of a single vessel (the umbilical cord) in the centre of a circular placenta of radius R, that is the case when no vessels are visible, can be solved exactly to give

$$p_1 = \frac{K^2 Q_1}{2\pi h\lambda} \left(\mathrm{K}_0(Kr) + \frac{\mathrm{K}_1(KR)}{\mathrm{I}_1(KR)} \mathrm{I}_0(Kr) \right), \tag{8.14}$$

$$\boldsymbol{u}_a = -\boldsymbol{u}_v = \frac{KQ_1}{2\pi h} \left(\mathrm{K}_1(Kr) - \frac{\mathrm{K}_1(KR)}{\mathrm{I}_1(KR)} \mathrm{I}_1(Kr) \right). \tag{8.15}$$

In this case we may estimate the pressure drop at the umbilical cord as

$$p_a|_{r=\rho_a} - p_a|_{r=\rho_v} = \frac{k_v \, p_1|_{r=\rho_a} + k_a \, p_1|_{r=\rho_v}}{k_a + k_v} \tag{8.16}$$

$$= \frac{\mu Q_1}{2\pi h} \left[\left(\frac{\mathrm{K}_0(K\rho_a)}{k_a} + \frac{\mathrm{K}_0(K\rho_v)}{k_v} \right) \right. $$
$$\left. + \frac{\mathrm{K}_1(KR)}{\mathrm{I}_1(KR)} \left(\frac{\mathrm{I}_0(K\rho_a)}{k_a} + \frac{\mathrm{I}_0(K\rho_v)}{k_v} \right) \right], \tag{8.17}$$

where ρ_a and ρ_v are respectively the radius of the arteries and vein in the umbilical cord (note we need to assume the two arteries are the same size for the model to work).

In order to understand this solution better, consider the case in which $KL \ll 1$ for typical length scales L within the placenta (note that this approximation is not yet justified). Using

$$\mathrm{I}_0(z) = 1 + O(z^2), \tag{8.18}$$

$$\mathrm{K}_0(z) = -\ln\left(\frac{z}{2}\right) - \gamma + O(z^2), \tag{8.19}$$

$$\mathrm{I}_1(z) = \frac{z}{2} + O(z^3), \tag{8.20}$$

$$\mathrm{K}_1(z) = \frac{1}{z} + O(z), \tag{8.21}$$

(Abramowitz & Stegun, 1964, equations 9.6.10–13), where γ is Euler's constant gives

$$p_1 \approx \frac{K^2 Q_1}{2\pi h\lambda}\left(\frac{2}{K^2 R^2} - \ln\left(\frac{Kr}{2}\right) - \gamma\right), \tag{8.22}$$

$$\boldsymbol{u}_a = -\boldsymbol{u}_v \approx \frac{Q_1}{2\pi r h}\left(1 - \frac{r^2}{R^2}\right). \tag{8.23}$$

Note that the non-zero divergence of $\boldsymbol{u}_a$ and $\boldsymbol{u}_v$, which represents transport from the arterial to the venous system, appears clearly in the second term in the bracket.

8.2.4   Method to find the solution in the case of a general placenta and vessels

In this section we set up a method to find numerical solutions of (8.9). Working in polar coordinates (r, θ) centred on the umbilical cord (actually it could be any point if preferred), we can write the general solution of (8.9) as

$$\tilde{p}_1 = \sum_{m=0}^{\infty} \mathrm{I}_m(Kr)\left(A_m \cos m\theta + B_m \sin m\theta\right) \tag{8.24}$$

where $A_m, B_m \in \mathbb{R}$, $B_0 = 0$. Numerically, it is not possible to work with the infinite series (8.24), and so we truncate at M terms:

$$\tilde{p}_1 = \sum_{m=0}^{M} \mathrm{I}_m(Kr)\left(A_m \cos m\theta + B_m \sin m\theta\right), \tag{8.25}$$

and thus we need to find $2M+1$ unknown constants A_m and B_m that satisfy the boundary condition (8.11) as closely as possible.

   We denote the locations of the ends of the terminal vessels by (X_i, Y_i) in Cartesian coordinates, and approximate the boundary of the placenta by a polygon with N_p vertices at the points (x_l, y_l), $l = 1, 2, \ldots, N_p$, which are arranged in anticlockwise order around the boundary. At the midpoint of the lth edge, the point

$$\boldsymbol{t}_{0l} = \left(\frac{x_l + x_{l+1}}{2}, \frac{y_l + y_{l+1}}{2}\right), \tag{8.26}$$

where we identify (x_{N_p+1}, y_{N_p+1}) with (x_1, y_1), the normal vector is given, respectively in Cartesian and polar coordinates, by

$$\hat{\boldsymbol{n}}_l = \frac{1}{R_l}\left(y_{l+1} - y_l, x_l - x_{l+1}\right)$$

$$= \frac{1}{r_{0l}R_l} \left(\left(x_l y_{l+1} - x_{l+1} y_l \right) \hat{\boldsymbol{r}} + \frac{1}{2} \left(x_l^2 - x_{l+1}^2 + y_l^2 - y_{l+1}^2 \right) \hat{\boldsymbol{\theta}} \right), \quad (8.27)$$

where $R_l = \sqrt{(x_{l+1} - x_l)^2 + (y_{l+1} - y_l)^2}$ is the distance between neighbouring vertices and $r_{0l} = |\boldsymbol{t}_{0l}|$. At this point the boundary condition (8.11) states

$$\frac{1}{r_{0l}R_l} \sum_{m=0}^{M} \mathbb{A}_{lm} + \frac{1}{2r_{0l}} \mathbb{B}_{lm} = \frac{K^3}{2\pi h \lambda R_l} \sum_{\text{vessels } i} \frac{Q_i}{r_{il}} \mathbb{X}_{il} \, \mathrm{K}_1 \left(K r_{il} \right), \quad (8.28)$$

where

$$\mathbb{A}_{lm} = \left(x_l y_{l+1} - x_{l+1} y_l \right) K \, \mathrm{I}'_m \left(K r_{0l} \right) \left(A_m \cos m\theta_{0l} + B_m \sin m\theta_{0l} \right) \quad (8.29)$$

$$\mathbb{B}_{lm} = \left(x_l^2 - x_{l+1}^2 + y_l^2 - y_{l+1}^2 \right) m \, \mathrm{I}_m \left(K r_{0l} \right)$$
$$\times \left(B_m \cos m\theta_{0l} - A_m \sin m\theta_{0l} \right) \quad (8.30)$$

$$\mathbb{X}_{il} = \left(\frac{x_l + x_{l+1}}{2} - X_i \right) \left(y_{l+1} - y_l \right) - \left(\frac{y_l + y_{l+1}}{2} - Y_i \right) \left(x_{l+1} - x_l \right) \quad (8.31)$$

and

$$\boldsymbol{t}_{il} = \left(\frac{x_l + x_{l+1}}{2} - X_i, \frac{y_l + y_{l+1}}{2} - Y_i \right) \quad (8.32)$$

is the vector from the ith vessel end to the lth midpoint, and $r_{il} = |\boldsymbol{t}_{il}|$, $\theta_{0l} = \arg(\boldsymbol{t}_{0l})$. Choosing $2M+1$ different values of l (for example by choosing $N_p = 2M + 1$ and using the midpoints of all the edges), we obtain $2M + 1$ linear equations (8.28) that can be used to determine the $2M + 1$ constants A_m and B_m. Substituting these into (8.25) gives an approximation for $\tilde{p}_1$, and hence we may use (8.13) and (8.12) to find the approximate pressure and flux per unit area in the arterial and venous networks.

8.3   Network model of the large vessels

We assume that we have an image of the major arteries (or equivalently of the veins, which we assume are following the same paths as the arteries). Suppose there are N_v arteries (or equivalently veins) on the image and number these from 1 to N_v, such that vessels 1 to N_u are attached directly to the umbilical cord, vessels $N_u + 1$ to N_{iv} are the other vessels that are not terminal and vessels $N_{iv} + 1$ to N_v are terminal. We assume that each bifurcation has one parent and two daughter vessels, that artery i has length L_i and diameters D_{ai} and therefore vein i also has length L_i and we denote its diameter by D_{vi}. We denote the two daughter vessels of vessel i by $d_1(i)$

and $d_2(i)$, where $d_{1,2} : \{1, 2, \ldots, N_{iv}\} \mapsto \{N_u + 1, N_u + 2, \ldots, N_v\}$ and the parent vessel of vessel i by $p(i)$, where $p : \{1, 2, \ldots, N_v\} \mapsto \{0, 1, \ldots, N_{iv}\}$ (we set $p(i) = 0$ for vessels $1, \ldots N_u$ that are attached to the umbilical cord). Thus $i = p(d_1(i)) = p(d_2(i))$ for $i = 1, \ldots, N_{iv}$ and i is equal to $d_1(p(i))$ or $d_2(p(i))$ for $i = N_u + 1, \ldots, N_v$.

We denote by Q_i the flux through the ith artery and by Q_0 the flux through the two arteries in the umbilical cord. Since the flux exiting the terminal artery equals that of the corresponding vein, the fluxes in vein i must equal Q_i over the whole network, and the flux in the vein in the umbilical cord equals Q_0. We let P_{ai} be the pressure at the distal (to the fetus) end of artery i ($i = 1, \ldots, N_v$) and P_{a0} be the pressure in the arteries in the umbilical cord (we assume the two arteries have equal pressures). and P_{vi} be the pressure in the distal end of vein i and P_{v0} be the pressure in the vein of the umbilical cord. We let $P_{ai} - P_{vi} = P_i$.

Mass conservation at the umbilical cord implies that

$$Q_0 = \sum_{i=1}^{N_u} Q_i, \tag{8.33}$$

and mass conservation at the distal end of the ith vessel implies

$$Q_i = Q_{d_1(i)} + Q_{d_2(i)}, \quad \text{for } i = 1, \ldots, N_{iv}. \tag{8.34}$$

The porous medium model provides the relationships

$$P_i = P_{ai} - P_{vi} = \sum_{j=N_{iv}+1}^{N_v} \Lambda_{ij} Q_j, \quad \text{for } i = N_{iv} + 1, \ldots, N_v, \tag{8.35}$$

where we solve for $\tilde{p}_1$ for the case $Q_k = \delta_{jk}$ (that is all the Q_k's are zero except Q_j, which equals 1), and set Λ_{ij} to be the value of p_1 at the ith vessel end, which, from (8.13), is

$$\Lambda_{ij} = \begin{cases} \tilde{p}_1|_{\text{vessel } i} + \dfrac{K^2}{2\pi h \lambda} \dfrac{k_v \, \mathrm{K}_0\left(\frac{1}{2}KD_{ai}\right) + k_a \, \mathrm{K}_0\left(\frac{1}{2}KD_{vi}\right)}{k_a + k_v} & \text{for } i = j, \\[2ex] \tilde{p}_1|_{\text{vessel } i} + \dfrac{K^2}{2\pi h \lambda} \, \mathrm{K}_0(Kr_{ij}) & \text{for } i \neq j, \end{cases} \tag{8.36}$$

where r_{ij} is the distance between the ith and jth vessel ends. Finally, momentum conservation in the ith artery and the ith vein gives respectively

$$P_{ap(i)} - P_{ai} = \Gamma_{ai} Q_i, \quad P_{vi} - P_{vp(i)} = \Gamma_{vi} Q_i, \quad \text{for } i = 1, \ldots, N_v, \tag{8.37}$$

where $\Gamma_{ai} = 128\mu L_i/\pi D_{ai}^4$ and $\Gamma_{vi} = 128\mu L_i/\pi D_{vi}^4$ are the Poiseuille resistances. Combining these

$$P_{p(i)} - P_i = \left(\Gamma_{ai} + \Gamma_{vi}\right) Q_i, \quad \text{for } i = 1, \ldots, N_v. \qquad (8.38)$$

Equations (8.33)–(8.35) and (8.38) represent $2N_v + 1$ linear equations for the $2N_v + 2$ variables P_i and Q_i, $i = 0, 1, \ldots, N_v$. Setting $P_0 = 1$ provides sufficient information to calculate Q_0. The value Q_0 thus calculated provides a measure of the conductivity of the placenta.

8.4   Parameter estimation

In order to use the model, certain parameters must be found, which are listed in this section. Using the image we can find the numbers of vessels N_u, N_{iv} and N_v, the relationships defining the bifurcations, $p(i)$, $d_1(i)$ and $d_2(i)$, and the lengths L_i. We also require measurements of the vessel diameters D_{ai} and D_{vi}, and these necessitate further image processing. In addition we need estimates of the blood viscosity, μ, the Darcy permeabilities, k_a and k_v, the flow rate per unit pressure drop, λ, and the placenta height, h.

Figure 13 shows the output of the numerical code on an idealised placenta, demonstrating the feasibility of the method. This is done with made-up parameter values. In future work we will estimate these parameters from the literature, and use them to predict the placental blood flow for images of real placentas.

8.5   Discussion

The porous medium model neglects several aspects of the placenta. Crucially the model assumes that arteries and veins lie along the same tracks, which is unlikely to be true in practice. A further complication is that each lobule is not necessarily supplied by either a single major artery and/or drained by a single vein. The assumption that arteries and veins are in the same place is likely to have a significant effect on the quantitative predictions of the model; nevertheless, there is likely to be a good correlation between the ranks of the efficiency predicted by the model and the true efficiency of the placenta. If it were possible to identify separately the arteries and veins on the image, this would significantly improve the predictive capability of the model.

In addition, currently the images do not include estimates of vessel diameters, and so this information must be estimated. Poiseuille's law shows the flux depends on the fourth power of the diameter for a given pressure
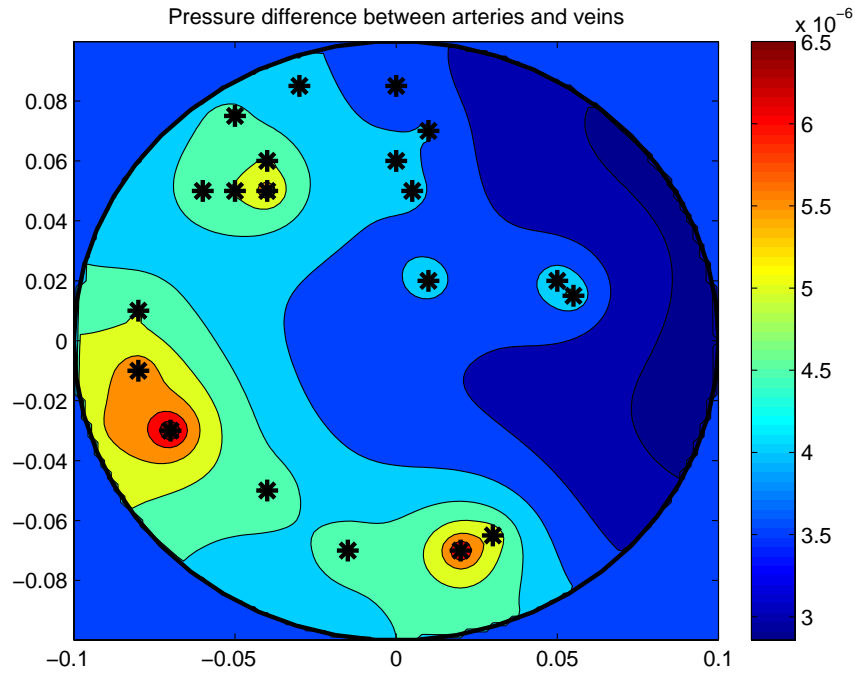
FIGURE 13: *Distribution of the pressure difference p_1 in an idealised placenta, based on a simplified version of the placenta in the file `NORMAL2`. The boundary of the idealised placenta (in this case a circle) is shown by the black line (using 51 vertices) and the approximate locations of the ends of the vessels are shown by the black asterisks. The parameter values used are $\mu = 0.004\,\mathrm{Pa\,s}$, $\lambda = 0.1\,(\mathrm{Pa\,s})^{-1}$, $k_a = k_v = 5 \times 10^{-5}\,\mathrm{m}^2$, $h = 3\,\mathrm{cm}$. Every vessel is treated as having length $2\,\mathrm{cm}$ and diameter $1\,\mathrm{mm}$*

drop, and so it is important to use an accurate estimate of the diameter of a vessel. The model also does not differentiate between the two arteries supplying the placenta, but this is unlikely to have a significant effect since the pressures of the blood in these vessels are similar. Currently we must estimate parameters of the network of vessels from the image of the placenta; however, in future work we plan to automate retrieval of the required parameters.

An interesting extension of this model would be to analyse the blood flow in the placentas of identical twins. Identical twins share a single placenta, and this can lead to the formation of anastomoses – vessels connecting the blood supplies of the two fetuses. These connections can be very dangerous

for the fetuses because these can have a large pressure drop along their length, leading to loss of blood from one fetus to the other. Franke *et al.* (2003) used a numerical model to estimate blood flow in the major vessels. They use a reflection condition at the downstream end of the vessels, but this could be made more accurate using a porous medium model.

9 Modelling the development of the villous tree

In this section, we propose a model for the normal growth and development of the human placenta. The objectives are to understand the abnormal patterns seen in complicated pregnancies. Background about the development of the villous tree can be found in §2.

9.1 Modelling the villi growth rate as linearly dependent on nutrients

A simple model is presented here on the growth of the placenta. The initial time is chosen to be when the placenta has differentiated into around 5 villi and has just started sending blockers into the spiral arteries immediately located opposite the villi. This is around time $t = 4$ weeks. Clinical observations suggest that the diameter of the surface covered by these villi is approximately 2 centimetres in diameter at that time. Assume that five villi of that size have formed already in a star shape as shown in figure 14. The radius and coordinates of the boundary is given by

$$r_{\text{villi}} = (0.3 + 0.15 \cos 5\theta) \,\text{cm}\,, \tag{9.1}$$

$$\begin{pmatrix} x \\ y \end{pmatrix} = (0.3 + 0.15 \cos 5\theta) \begin{pmatrix} \cos \theta \\ \sin \theta \end{pmatrix} \,\text{cm}\,. \tag{9.2}$$

For the next 6 weeks the uterus grows in order to accommodate for the developing fetus. The model assumes that this growth is independent of the development of the placenta and the parameters are chosen to represent a uterus of size $5 \times 5 \times 5 \,\text{cm}^3$ in week 4 and $10 \times 10 \times 7 \,\text{cm}^3$ in week 10. These values are based on clinical observations. The radius of the uterus is thus defined by

$$r_{\text{uterus}}(t) = \left(2.5 + (5 - 2.5) \frac{t/\,\text{weeks} - 4}{6} \right) \,\text{cm}\,, \tag{9.3}$$

where t is measured in weeks.

The diameter of the placenta is taken to be around $2 \,\text{cm}$ in diameter in week 4 and 4–$5 \,\text{cm}$ in week 10. The villi send blockers into the spiral arteries thus blocking most nutrients immediately below them. It is assumed that there are sufficient fats/sugars in the decidua that the growth of already-formed villi can be supported. The rate of growth or differentiation is chosen to be linearly dependent on the amount of nutrients in the system, with these being uniformly distributed in the space around the placenta. The shape
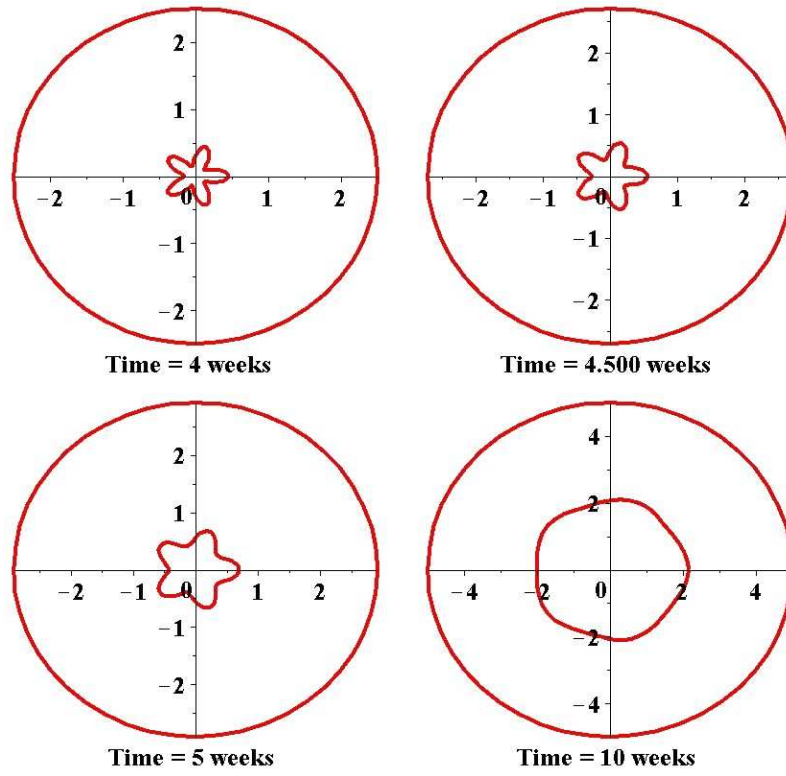
FIGURE 14: *Development of villi in the placenta and the surface of the uterus, which is covered by spiral arteries delivering nutrients uniformly to the placenta, between the 4th and 10th weeks of pregnancy.*

and structure of the uterus is very complicated. For simplicity, it will be assumed that the embryo is in a position in the uterus where, by symmetry, it receives the same nutrients in all directions. This can be modelled by saying the surface of the uterus, which is covered by spiral arteries delivering nutrients to the placenta, is circular with the villi positioned in its centre.

A plot of the solution to the problem described above is given in figure 14. This together with several other solutions show that regardless of the initial condition or the number of villi at time $t = 4$ weeks, the solution tends towards a circular shape and remains in the centre of the uterine domain. This is physically realistic as the placenta would maximise its nutrition uptake with time. The growth rates have been chosen to match clinical observations assuming a healthy placenta and uterus so the model does not provide any information about the growth size. Consider, however, a uterus

that deliver more nutrients on one side rather than another to the placenta. For simplicity, consider such a case where the uterus is still circular but the position of the placenta is off its centre. The initial condition of the villi is then given by

$$\begin{pmatrix} x \\ y \end{pmatrix} = \begin{pmatrix} x_0 \\ y_0 \end{pmatrix} + (0.3 + 0.15 \cos 5\theta) \begin{pmatrix} \cos \theta \\ \sin \theta \end{pmatrix} \text{cm}. \tag{9.4}$$

Such a solution is shown in figure 15 for the off-centre values $x_0 = 0.7$, $y_0 = -1.9$. It shows that the villi tend towards a circular shape but do not manage to reach that by the 10th week and remains as an elliptical shape. The size of the placenta at the final time is slightly smaller than that in the solution in figure 14, but is still of similar magnitude. There are clinical observations of placentas that are elliptical in shape and smaller in size that perform worse than those that are regular. So the hypothesis that the function of the placenta may decline due to an irregular development of the villi is worth considering further. However, many assumptions have been made in this model that need revising. These include the circular shape of the uterus, the immediate deactivation of the spiral arteries, the linear growth relationship of the placenta to the nutrients in the system and the uniform distribution of nutrients in the decidua around the spiral arteries. An attempt to develop a more sophisticated model was made during the study group but was not finished due to time restrictions. A brief overview is presented next.

9.2 Modelling the development of the villi using chemotaxis and diffusion

9.2.1 General equations

The shape of the uterus is modelled as growing linearly in time again with the same rate and form as in (9.3). However, the difference in this model is that the growth of the placenta is not assumed to be linearly proportional to uniformly-distributed nutrients in the decidua, but is driven by chemotaxis toward areas of high concentration of these. The decidua can be modelled as consisting of nutritional sources and sinks, representing the spiral arteries and maternal veins. Let these positions be labelled as $\boldsymbol{x}_n$ for the sources and $\boldsymbol{y}_n$ for the sinks. Let $T(x, y, t)$ be the cells on the embryonic side that are forming villi, $T_c(x, y, t)$ the position of the boundary of the $T(x, y, t)$-cells and let $a(x, y, t)$ be the concentration of nutrients in the decidua. Then a
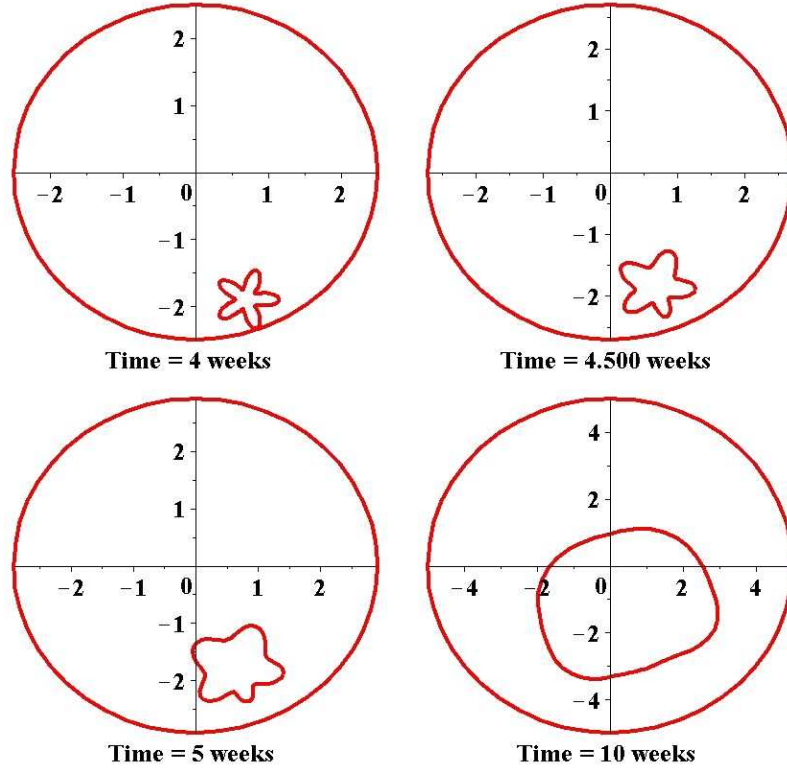
FIGURE 15: *Development of villi in the placenta and the surface of the uterus, which is covered by spiral arteries delivering nutrients to the placenta in a non-uniform way, between the 4th and 10th weeks of pregnancy.*

set of differential equations that can describe the system is

$$\frac{\partial a}{\partial t} = D_1 \nabla^2 a + \sum_n k_n f_n(\boldsymbol{x}_n, T_c)\, \delta\left(\boldsymbol{x} - \boldsymbol{x}_n\right)$$

$$- \sum_m l_m\, g_m(\boldsymbol{x}_m, T_c)\, \delta\left(\boldsymbol{x} - \boldsymbol{y}_m\right) - c_1(a) - c_2(T)\,, \quad (9.5)$$

$$\frac{\partial T}{\partial t} = D_2 \nabla^2 T - \boldsymbol{\nabla} \cdot (\chi T \boldsymbol{\nabla} a) - c_3(T) + c_4(T)\,. \quad (9.6)$$

The constants $D_{1,2}$ are the diffusion rates for the distributions $a(x, y, t)$ and $T(x, y, t)$ respectively. The constants k_n and l_m represent the strength in nutrients either delivered by the nth spiral artery or taken up by the mth vein. Both sink and sources are modelled as delta functions of different signs. This is an assumption and it should be considered that other singularities
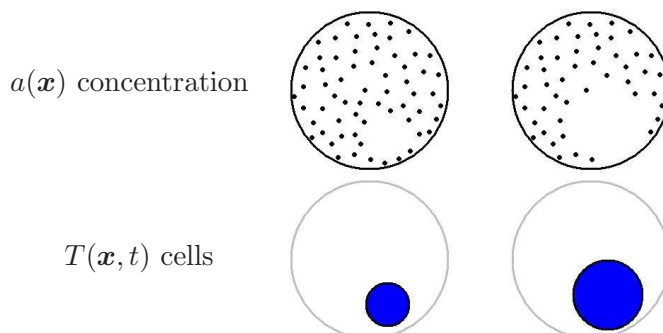
$a(\boldsymbol{x})$ concentration

$T(\boldsymbol{x}, t)$ cells

FIGURE 16: *A diagram of the spiral arteries being blocked by hormones sent from the villi. This process is modelled by switching off all spiral arteries covered by the villous cells. The black outline in the second row represents the boundary of these cells T_c. The dots in the first row represent positions of spiral arteries.*

might give better results. The strength of 'attraction' of the villous cells toward nutrients is measured by the chemotactic term χ. This can be a function of space, but for simplicity will be assumed to be constant. The functions $c_1(a)$ and $c_2(T)$ represent oxygen uptake by the decidual tissue and villous cells respectively. The terms $c_3(T)$ and $c_4(T)$ are the death and birth rates of the $T(x, y, t)$-cells. These can probably be neglected without much change in the solution since the growth is modelled by the diffusion rather than by the number of villi. Finally, the function $f_n(\boldsymbol{x}_n, T_c)$ is the non-linear term in the equations that represents the blocking and unblocking of spiral arteries and maternal veins. It has the property that it is 0 when the hormones have been released to block the arteries directly underneath the villi and 1 when they have not. Mathematically, it can be represented as

$$f_n(\boldsymbol{x}_n, T_c) = \begin{cases} 1 & : \quad \boldsymbol{x}_n \notin T_c, \\ 0 & : \quad \boldsymbol{x}_n \in T_c. \end{cases} \tag{9.7}$$

The term g_m is similar to f_n but relates to the maternal veins rather than spiral arteries. Both their functions are described by the diagram in figure 16.

9.2.2   First simplification

To make progress we consider the following simplifications to the problem. The terms $c_{2,3,4}(T)$ in (9.5)–(9.6) represent processes that will change the

solution quantitatively rather than qualitatively and also are not the key ones in the problem to be modelled. An uptake term $c_1(a)$ is needed in the first equation to balance the diffusion term. Thus they can be neglected. The simplest possible form that can be taken is a linear relationship in $a(x, y, t)$. However, other forms should also be considered in the future. In addition, the oxygen concentration can be assumed to be steady in time as it is assumed that the spatial distribution will not vary greatly in time. This assumption is realistic for short timescales when the uterus is of constant size and the locations of the sources and sinks do not change. Then the system of equations can be simplified to

$$0 = D_1 \, \nabla^2 a + \sum_n k_n f_n(\boldsymbol{x}_n, T_c) \delta\left(\boldsymbol{x} - \boldsymbol{x}_n\right)$$

$$- \sum_m l_m g_m(\boldsymbol{x}_m, T_c) \delta\left(\boldsymbol{x} - \boldsymbol{y}_m\right) - c_1 a \,, \qquad (9.8)$$

$$\frac{\partial T}{\partial t} = D_2 \, \nabla^2 T - \boldsymbol{\nabla} \cdot (\chi T \boldsymbol{\nabla} a) \,, \qquad (9.9)$$

where c_1 is the rate of uptake. The first equation in this system is non-linear but can be solved as a linear problem at each time-step. This means that it is possible to obtain a solution for the oxygen distribution by taking the effect of diffusion and a single source term and then linearly adding all sources together at every time step. Without loss of generality, consider all sinks to be 0 and that the sources can also represent sinks if the strength constants k_n can be taken to be negative.

9.2.3   Nutrient concentration with a single central source

Consider a source singularity in two-dimensional space that produces a concentration of nutrients that satisfy

$$0 = D_1 \, \nabla^2 a - c_1 a \,, \qquad (9.10)$$

subject to $\partial a / \partial r = 0$ at $r = 1$ and a singularity condition at $r = 0$ such that the flux through that point is some constant Q. The general solution to (9.10) is

$$a(x, y) = A \, \mathrm{I}_0 \left(\sqrt{\frac{c_1}{D_1}} r \right) + B \, \mathrm{K}_0 \left(\sqrt{\frac{c_1}{D_1}} r \right) \,, \qquad (9.11)$$

where I_0 and K_0 are modified Bessel functions of the first and second kind respectively.

The boundary condition then yields

$$A = B \frac{K_1\left(\sqrt{\frac{c_1}{D_1}}\right)}{I_1\left(\sqrt{\frac{c_1}{D_1}}\right)}.$$ (9.12)

Finally, the flux condition gives

$$\oint (-\boldsymbol{\nabla} a)\cdot\boldsymbol{n}\,\mathrm{d}l = Q \qquad \Rightarrow \qquad Q = -\lim_{\epsilon\to 0}\int_0^{2\pi} \frac{\partial a}{\partial r}\bigg|_{r=\epsilon}\epsilon\,\mathrm{d}\theta = 2\pi B\,,$$ (9.13)

which determines the constant B and yields a full solution. Solving the same problem for a general source that is not at $r = 0$ is a lot harder and was not done during the study group. There was an idea to change the coordinate system from (r,θ) to one with an origin at the source and the hope that the boundary condition will work out, but that analysis was not finished due to time constraints.

9.2.4   Nutrient concentration with a single off-centre source

A third attempt was made to solve the following problem

$$0 = D_1\nabla^2 a - c_1 a + Q\,\delta(r-R)\,\delta(\theta-\Theta)$$ (9.14)

$$|\boldsymbol{\nabla} a| \to 0 \quad \text{as} \quad r \to 0\,,$$ (9.15)

$$\frac{\partial a}{\partial r} = 0 \quad \text{at} \quad r = 1\,.$$ (9.16)

Using separation of variables the general solution to the homogeneous version of (9.14) (i.e. with Q=0) is

$$a(r,\theta) = \sum_n \left[A_n\,\mathrm{I}_n\left(\sqrt{\frac{c_1}{D_1}}r\right) + B_n\,\mathrm{K}_n\left(\sqrt{\frac{c_1}{D_1}}r\right)\right]$$
$$\times \left(C_n\sin(n\theta) + D_n\cos(n\theta)\right).$$ (9.17)

We then consider separate solutions based on (9.17) in $0 < r < R$ and $R < r < 1$, and apply the matching conditions

$$[\,a\,]_{R-}^{R+} = 0\,,$$ (9.18)

$$\left[\frac{\partial a}{\partial r}\right]_{R-}^{R+} = -\frac{Q}{D_1}\,\delta(\theta-\Theta)\,.$$ (9.19)

Applying the boundary conditions (9.15) and (9.16) together with the first matching condition (9.18) and ensuring symmetry about $\theta = \Theta$, we obtain

$$
a(r,\theta) = \begin{cases} \frac{1}{2}a_0\,f_0(r)\,g_0(R) + \displaystyle\sum_{n=1}^{\infty} a_n\,f_n(r)\,g_n(R)\,\cos\Big(n(\theta-\Theta)\Big) & : \quad r < R \\[2ex] \frac{1}{2}a_0\,f_0(R)\,g_0(r) + \displaystyle\sum_{n=1}^{\infty} a_n\,f_n(R)\,g_n(r)\,\cos\Big(n(\theta-\Theta)\Big) & : \quad r > R \end{cases}
$$

$$(9.20)$$

where

$$
f_n(r) = \mathrm{I}_n\left(\sqrt{\frac{c_1}{D_1}}\,r\right)\,,
$$

$$(9.21)$$

$$
g_n(r) = \frac{\mathrm{I}_n\left(\sqrt{\frac{c_1}{D_1}}r\right)}{\mathrm{I}'_n\left(\sqrt{\frac{c_1}{D_1}}\right)} - \frac{\mathrm{K}_n\left(\sqrt{\frac{c_1}{D_1}}r\right)}{\mathrm{K}'_n\left(\sqrt{\frac{c_1}{D_1}}\right)}\,.
$$

$$(9.22)$$

The a_n are determined by applying the final matching condition (9.19). In what reduces to finding the Fourier series for $\delta(\theta - \Theta)$, we obtain

$$
a_n = \frac{-Q}{\pi D_1}\Big(f_n(R)g'_n(R) - f'_n(R)g_n(R)\Big)^{-1}\,.
$$

$$(9.23)$$

9.2.5   Multiple off-centre sources

In principal, a solution could now be built for multiple sources, by superposing a number of copies of this solution with different values of Q, Θ, R. However, owing to a lack of time, there was no further investigation of this at the study group.

The main problem faced when deciding what the model should be was the fact that it was not obvious what singularity or distribution is most realistic. In the analysis that the research group did when modelling the branching of blood vessels a Gaussian distribution was chosen. In this model it seemed easier to choose Dirac delta functions to attempt the analysis. Lots of future work is needed in all areas of this project.

10 A stochastic model for the early development of the placenta

10.1 Model description

The model which we will go on to describe and implement in this section, is based on a number of assumptions, and aims to give some evidence for the following hypothesis; early development of the placenta is defined by the growth of the blood vessels from the attachment of the umbilical cord (which will become the chorionic plate arteries), and the direction of growth is driven by the gradient of a growth factor (possibly O_2). We also assume that this growth factor has diffused from point sources on the surface of the uterus, from the spiral arteries which will, at this stage, have become blocked by the presence of the fetus and placenta.

We also assume that the tips of the blood vessels are absorbing this growth factor, also by diffusion. It would be reasonable to expect the whole length of the blood vessel to absorb this, but for the purposes of this simple model we negated this.

Together, these sources and sinks of the growth factor give us a function of the density of the growth factor. If we assume that the diffusive effects cause each of these sources/sinks to have an approximate Gaussian distribution (corresponding to our assumption of blocked spiral arteries being the point and temporal sources of growth factor), and that the blood vessels are drawn to areas of high oxygen concentration, then the potential function for each vessel tip x_p is given by

$$V_p(x) = -\sum_{n=1}^{N} A_n \exp\left(-\frac{1}{2\sigma_{GF}^2}|x - y_n|^2\right)$$
$$+ \sum_{i \neq p}^{P} A_{GF} \exp\left(-\frac{1}{2\sigma_{GF}^2}|x - x_i|^2\right), \qquad (10.1)$$

where the y_n are the positions of the sources of the growth factor (corresponding to spiral arteries on the surface of the uterus), σ_{GF} is the standard deviation of the density of growth factor due to diffusion in the tissue, and the A_n are the amplitudes of the sources of the growth factor, and A_{GF} is the amplitude of absorption of the growth factor of each of the blood vessel tips. Because diffusion is property of the material (tissue), both sources and sinks have the same value of σ_{GF}.

We assume that since the cells in the uterus are able to sense changes of concentration of the growth factor over their length, that they are able to

estimate which direction has an increasing density of the growth factor (or in other words, estimate the gradient of the potential function V_p).

However, since they are only able to estimate this value and may be sensitive to small variations in the tissue and the growth factor's ability to diffuse through it, it is also safe to assume that there is some error in this estimation. We will model this through inclusion of stochastic terms in the dynamics of the blood vessel tips. Consider the following Langevin equation for a Brownian particle moving in a potential landscape V_p:

$$\mathrm{d}x_p = -\nabla V_p(x_p) + D\,\mathrm{d}W \tag{10.2}$$

If we model each of the blood vessel tips in such a way, we end up with a system of P coupled stochastic differential equations (SDEs). In general the particles will migrate to regions near the sources, but they will also repel each other. These types of equations are easily implemented on a computer, using the Euler–Marayama discretization. That is, at each time step we compute

$$x_p(t + \Delta t) = x_p - \Delta t\,\nabla V_p(x_p) + D\sqrt{\Delta t}\,\xi\,, \tag{10.3}$$

where the ξ are independent identically distributed $\mathcal{N}(0,1)$ random variables. This method has $O(\Delta t)$ error.

Once we have this model for the dynamics of the vessel tips, we also need to consider what conditions need to be present for vessels to branch. It seems sensible that branching should only occur if there is a profusion of GF, since there is little point in growing vasculature to regions with no GF. Therefore, we assert that branching can only occur if the local density of GF is above a certain threshold, and therefore the value of the potential is below a certain threshold, which we denote F.

Moreover, we would expect branching to occur when the blood vessel has less information about which direction is the best to search for sources of GF which should correspond to the case when there are two sources apart at similar distance from the growing tip. This will occur when the gradient of the potential is small. Therefore we implement the following branching condition:

$$\mathbb{P}(x_p \text{ branches in } [t, t + \Delta t] | V_p(x_p) < F) =$$
$$\min\left\{1, \Delta t \exp\left(L\left(\frac{\delta}{\|\mathrm{grad}V(x_p)\|^2} - 1\right)\right)\right\}, \tag{10.4}$$

else if $V_p(x_p) \geq F$, the probability is zero.

Now all that remains is to define our parameter values and initial conditions that we used in our simulations.

$$
\begin{aligned}
A_{GF} &= 1.0, & \sigma_{GF} &= 0.8, \\
P_0 &= 2, & P_T &= 20, \\
D &= 2 \times 10^{-2}, & L &= 1.4, \\
\delta &= 1 \times 10^{-5}, & F &= -2.0, \\
\Delta t &= 1 \times 10^{-2}, & \epsilon &= 5 \times 10^{-2}.
\end{aligned}
\tag{10.5}
$$

Here P_0 is the initial number of blood vessel tips that start at the umbilical cord. We pick this number since this is the number of arteries present in the umbilical cord. All other parameters were picked using trial and error - realistic choice of parameters is definitely an area for further consideration.

P_T is the required number of terminations (i.e. spiral arteries reached by vessel tips) before the growth of blood vessels stops. A blood vessel terminates if it passes within a distance ϵ of a spiral artery.

As default, the cord is placed at $(0,0)$, and spiral arteries are placed at all points in the state space with integer coordinates, up to some maximum absolute value. In the computations that follow, this maximum was picked to be 10, since this gave us 436 spiral arteries, far more than are required before P_T terminations are reached.

10.2   Simulation results

Our hypothesis suggests that the placement of cord insertion is affected by the local oxygen densities around the cord. For example, if one spiral artery was missing/faulty, we would expect the arteries to grow in the opposite direction, up the gradient of oxygen density. The following pictures will show different abnormalities in placentas, the spiral artery configuration which we hypothesise might cause this effect, and the results of the simulation using that configuration.

First we consider a normal placenta. Figure 5(a) shows a trace of normal healthy placenta, with the cord insertion nicely in the centre of mass. Figure 17(a) shows the distribution of the spiral arteries, the sources of the GF, denoted by the green circles. The cord is denoted by the black circle. Figure 17(b) shows the results of a simulation of the model with this configuration.

Next we consider placentas with lateral cord insertions, an example of which is given in figures 3(b) and 5(b). If we were to switch off one spiral artery close to the cord, then the blood vessels (assuming our hypothesis has some weight) will grow away from this region. Figure 18(a) shows a
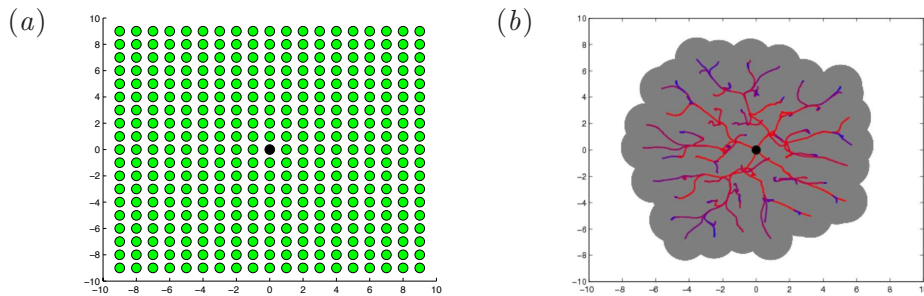
FIGURE 17: *(a) Normal configuration of the spiral arteries (green circles) around the umbilical cord (black circle). (b) Results of the simulation with this configuration.*
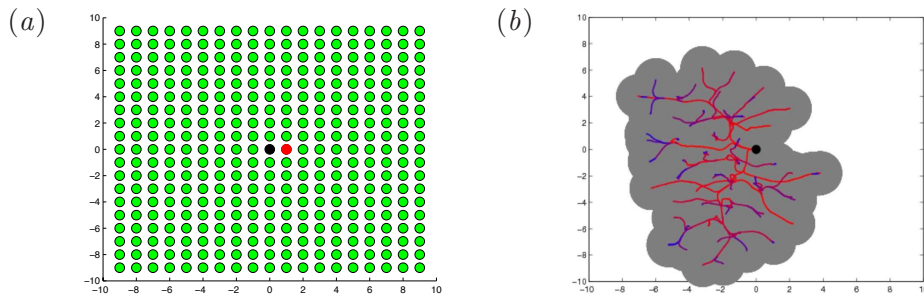

FIGURE 18: *(a) Configuration of spiral arteries causing a lateral cord insertion. (b) Results of the simulation with this configuration.*

possible configuration which could cause such an effect (spiral arteries that have been switched off are denoted by red circles), and figure 18(b) shows the results of a simulation with this configuration. It can be seen from this picture that the cord insertion in this case is indeed off-centre. We have also created figures with more spiral arteries switched off on one side which cause even more extreme lateral cord insertions.

Finally, we consider bipartite placentas. An example of such a placenta is given in figure 4, where the placenta appears to be made of two sections joining along one side. Figure 19(a) gives a possible configuration which might cause this kind of effect, and figure 19(b) shows a simulation which we got using this configuration.
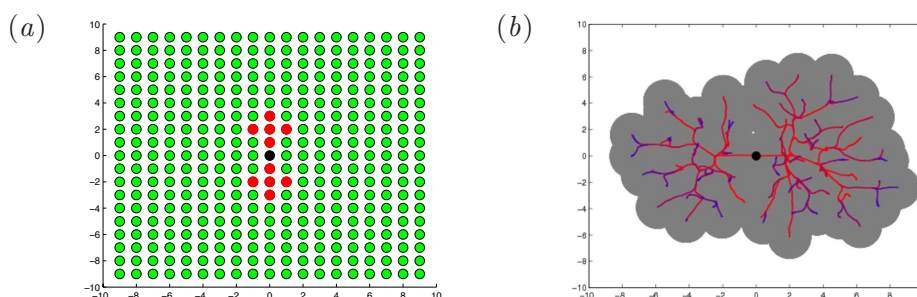
FIGURE 19: *(a) Configuration of spiral arteries causing growth of bipartite placenta. (b) Results of the simulation with this configuration.*

10.3 Conclusions

We have made a hypothesis as to one possible cause for abnormal shapes of placenta. We have formulated a model based upon this hypothesis, and were able to recreate the lateral cord insertion and bipartite placenta abnormalities. This model is clearly only a first approximation, but it does go to show that the proliferation and distribution of some kind of growth factor in the very early stages of pregnancy could be a cause of these abnormalities. Since these abnormalities in our model are caused by a lack of a decent uniform blood supply in the uterus, this could go some way to give a possible explanation as to the link between abnormal placental shapes and restricted fetal growth and still-birth. They could all be symptoms of an insufficient blood supply which as the fetus reaches the latter stages of pregnancy requires an increasing amount of nutrition which cannot be met by the substandard supply.

Also, we postulate that the final shape of discoid placenta is given by the grown vascular tree. Even-though the modelled vascular tree does contain only main vessels and not capillaries, we assume that the tissue of placenta itself can survive (and grow eventually) only in some region around the main vessels. This region could possibly be determined by distance from the vessels that would correspond to penetration depth of oxygen by diffusion in the living tissue. Actually, this distance is around $60\,\mu$m which corresponds well to 4-cell thick layer of placenta tissue that survives on the degrading side of spherical placenta opposite from umbilical cord.

In terms of further work on this model, there are many things we could look at. One would be the use of Gaussians as the approximations of the diffusion of the GF. This approximation is fine if we assume that there is

not a constant supply of GF from the source (this seems reasonable as the spiral arteries become blocked at this stage of the pregnancy so there is no significant blood flow here). However, if we assume that the spiral arteries are constantly diffusing GF into the placental region then we would need to solve a differential equation for the evolution of the concentration of GF.

Also, since the simulations are of a stochastic nature, simply finding one simulation that produces a picture which matches the pictures of abnormal placentas is not sufficient, since every simulation will give us a different placenta. Ideally we would produce many many realisations of the placenta for each configuration and estimate a probability density for the vascular network. The shape of this probability distribution will give us a better indication of the impact of the distribution of the spiral arteries.

We are also interested in matching statistics from the real placentas (numbers of branches, average branch length, average branching angle etc) with the results from the model in different scenarios. By verifying that certain features are present in both the statistics and the model, we add further evidence to our hypothesis.

11 Model for the formation and growth of vascular trees

In this section we outline an alternative probabilistic simulation method to model the formation of vascular trees. This is currently only at a very preliminary stage of development.

11.1 Problem description

We focus on the growth of the vascular network from the umbilical cord to the chorionic villi. Villi are small projections from mucous membranes. The chorion is one of the membranes that exist during pregnancy between the developing fetus and the mother. The chorionic villi come out of the chorion and go into the endometrium allowing nutrients to be transferred to fetal blood from the mother's blood (Wikipedia Contributors, 2010). We also aim to investigate the efficiency of vascular systems in terms of the blood supply under different umbilical cord insertion positions relative to the body of the placenta. We shall call a placenta with central umbilical chord insertion position a "normal" placenta and one with an umbilical cord insertion position at the side a "lateral" placenta.

The villi contain a capillary network consisting of "many closed circuits
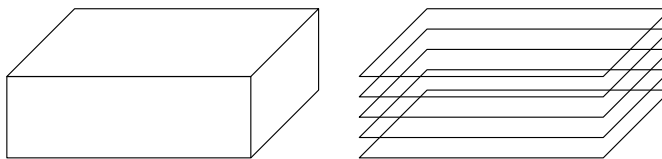
FIGURE 20: *Placenta grown space as a 3D object*

of blood vessels with no obvious source of blood flow". On the other hand the vascular network of the placenta has a source of blood flow (the umbilical chord) and consists of bifurcating vessels with directional blood flow. The process of transformation of the capillary network to the branching structure is believed to involve a process of selecting some capillaries from the pre-existing ones (Geva *et al.*, 2002).

11.2   Model of growth

For simulation purposes we model the placental growth space as an three-dimensional object as in figure 20 which consists of a large number of horizontal slices. However this is just an artifact to model the growth of the vascular structure on the two dimensional top surface of the placenta. The resulting vascular tree in two dimensions is the two dimensional view of the three dimensional object viewed from above (figure 21). This can be regarded as a branching process on the placental surface.

11.3   Outline of algorithm

We propose the following stochastic simulation algorithm for building up the vascular tree:

1. Start with a single point at the umbilical chord. At each stage choose several points in the layer underneath according to a given probability distribution. Initially we would use a uniform distribution. However in real life there is a tendency for the vascular network to grow outward from the umbilical cord and a uniform distribution would not capture this and would give a very tangled network and as we want the network to spread outward from the centre a spatially non-homogeneous distribution with more weight at the edges would probably give a more realistic structure. The proposed vascular network would join the original point in the first layer to the points beneath in the second layer (see figure 21).
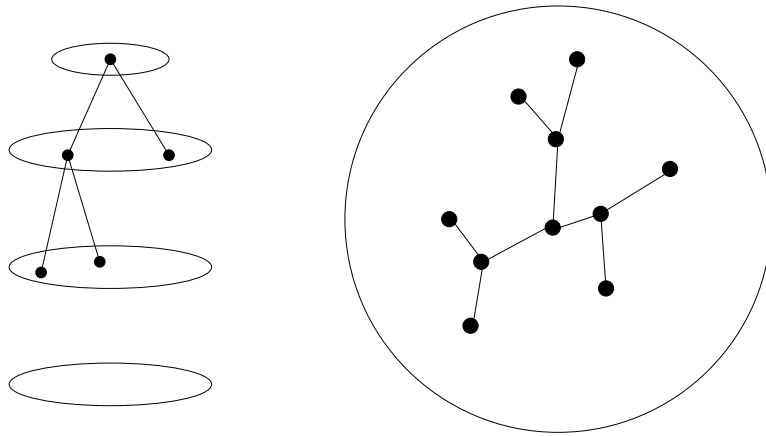
Figure 21: *Illustration of the Algorithm*

2. At the next stage we would use each of the points in the second layer as the roots of the tree and the same algorithm to generate more points in the third layer.

3. Then we would use each point in the new third layer to generate the fourth layer and so on.

4. At the end we wish the vascular tree to connect to the spiral arteries. Hence we connect every terminal section to one of the spiral arteries near it. If there are no spiral arteries sufficiently close then we decide that the probabilistic simulation is not feasible, delete the structure and try again.

If all of the spiral arteries are present then we would expect a normal placenta. If some are blocked then we would expect a pathologically-shaped placenta, for example a 'lateral' placenta, or possibly a non-circular placental shape.

Intuitively our idea is that building up a simulation model in this way may mimic how real placental vascular structures develop. The following diagram outlines the simulation procedure. At each stage we progressively build up the vascular network by adding more points (see the left-hand side of figure 21). The vascular network as viewed from above is shown on the right-hand side of figure 21.

We have started to write preliminary programs to perform the simulations but they are not yet complete.

Part IV
Conclusions and Future Work

12 Conclusions and future work

The placenta is known to be key to successful pregnancy outcomes yet it is both practically and ethically problematic to investigate in utero. As a result we are, at present, limited to considering 2 dimensional projections of full term placentas and, potentially, in the not too distant future, 2 dimensional scans of in utero placentas.

If we are to understand the risks caused by abnormal placentas we must have some means of making meaningful comparisons between placentas and linking them to pregnancy outcomes. We have proposed a variety of measures which are both replicable and sufficiently straightforward for a researcher to process rapidly and consistently. They require some refinement and a greater understanding of their sensitivity to the process of transforming a placental photograph into a trace. With such an understanding a protocol for trace production would offer a means of collating information of placentas suitable for large scale studies with sufficient statistical power to offer meaningful insights into the risks posed by abnormal placentas.

Whilst we cannot yet quantify the risk posed by abnormal placental topology, it is clear that irregularities are associated with poor pregnancy outcomes so the other approach of this project was in trying to understand the factors which might increase the risk of developing an abnormal placenta. Since it is not possible to perform in utero experiments, modelling is a powerful tool for investigating some of the possible mechanisms behind suboptimal development.

We have proposed a several different measures of placental shape, cord offset, and the efficiency of the vascular network. We now aim to systematically compute these measures for placentas from a larger data-set, and then see if they are correlated with pregnancy outcome. Such correlations will help our understanding of the role placenta shape and form may play in supporting pregnancy. If measurements of the placenta can be conducted

in utero, then our findings could also help to predict those at greater risk from complications.

We have proposed a variety of models which consider the development of the villous tree and which offer a potential explanation for deviations from the normal discoid shape and symmetric, bipartite arterial tree. The development is, in all cases limited due to time constraints. However, initial results suggest that they have sufficient potential to merit further work, particularly with regard to validation and parameter estimation.

Part V
Appendices

A Matlab code for image analysis and moment-based measures

The Matlab code used for the image analysis and momdent-based measure, as described in §5 is included below:

```matlab
function [Area,dcm,alpha,beta,lambda,gamma] = placenta_stats(picname)

% * picname is a string, eg. picname = 'DFM2COL.tif'; and it must be
%   in the folder this function is run from or the path must be
%   supplied.

% * Area returns the area of the placenta in cm^2.
% * dcm is the distance between the centre of mass of the cord and
%   the placenta in cm.
% * alpha, beta, gamma and lambda are as discussed in the report.


% Read in image
I=imread(picname);
I = im2double(I);
Iedge = I(:,:,1);
Ivessel = I(:,:,2);
Icord = I(:,:,3);
Iscale = max(0,I(:,:,4)-Iedge-Ivessel-Icord);

% Threshold, force pixel values to be 0 or 1
Iedge = im2bw(Iedge,0.5);
Ivessel = im2bw(Ivessel,0.5);
Icord = im2bw(Icord,0.5);
Iscale = im2bw(Iscale,0.5);

% Uncomment plots to check pictures loaded correctly
figure, imshow(Iscale)
```

```matlab
figure, imshow(Iedge)
figure, imshow(Ivessel)
figure, imshow(Icord)

% Fill placental outline
Iedge_fill = imfill(Iedge,'holes');
%figure, imshow(Iedge_fill)


% no of pixels in placenta
NP_area = sum(sum(Iedge_fill));
% length of scale bar ASSUMES PARRALLEL to edge of image and
% HORIZONTAL
[bin,j] = find(Iscale);
NP_scale = max(j)-min(j)+1;
% For a scale bar of 5cm, length of one pixel in cm
pix_length = 5/NP_scale;
Area = NP_area*pix_length^2;
% Length to normalise by in pixels
Norm_length = sqrt(NP_area/pi);


% Calculate centre of mass of placenta
[ip,jp] = find(Iedge_fill);
ipcom = sum(ip)/NP_area;
jpcom = sum(jp)/NP_area;
% Plot to check
Iedge_fill(floor(ipcom),floor(jpcom))=0;
%figure, imshow(Iedge_fill)


% Centre of mass of cord
[ic,jc] = find(Icord);
NP_cord = length(ic);
iccom = sum(ic)/NP_cord;
jccom = sum(jc)/NP_cord;


% Plot to check
Disp = Iedge_fill;
Disp(Icord)=0;
Disp(floor(iccom),floor(jccom))=1;
figure, imshow(Disp)


% Distance of com of cord from com of placenta
d = (iccom-ipcom)^2 + (jccom-jpcom)^2;
d = sqrt(d);
% in cm
```

```matlab
dcm = pix_length*d;


%Rob's measures
alpha = d/Norm_length;
sigma_sq = sum(ip.^2 + jp.^2)/NP_area -ipcom^2 -jpcom^2;
beta = 2*pi*sigma_sq/NP_area -1;
beta = sqrt(beta);

sig_xx = sum(ip.^2)/NP_area -ipcom^2;
sig_yy = sum(jp.^2)/NP_area -jpcom^2;
sig_xy = sum(ip.*jp)/NP_area -ipcom*jpcom;

M = [sig_xx, sig_xy; sig_xy, sig_yy];
evalues = eig(M);
lambda = sqrt(max(evalues)/min(evalues));

sig_a = sqrt(evalues(1));
sig_b = sqrt(evalues(2));

gamma = 4*pi*sig_a*sig_b/NP_area -1;
gamma = sqrt(gamma);
```

B   Proofs that β and γ are minimised by placentas with circular and elliptical cross-sections

Without loss of generality we choose our coordinate system so that the centre of mass of the placenta is at the origin, and the principal axes (i.e. the eigenvectors of $\mathbf{C}$) correspond to the x and y axes. We represent the boundary of a general placenta parametrically by considering it as an ellipse plus a perturbation:[1]

$$\begin{pmatrix} x \\ y \end{pmatrix} = \begin{pmatrix} X(t) \\ Y(t) \end{pmatrix} \equiv \begin{pmatrix} a\cos t \\ b\sin t \end{pmatrix} \left(1 + f(t)\right), \tag{B.1}$$

where $f(t) > -1$.

A general area integral over the placenta can be written as

$$I[g] = \iint g(x,y)\, \mathrm{d}A. \tag{B.2}$$

---

[1]This representation is not completely general since it excludes some more convoluted shapes, but it will suffice for our purposes.

Using the coordinate transformation

$$x = a\,\xi\cos t \tag{B.3}$$
$$y = b\,\xi\sin t \tag{B.4}$$

which has Jacobian $J = ab\xi$, we can rewrite the integral as

$$I[g] = ab \int_0^{2\pi} \int_0^{1+f(t)} g(a\,\xi\cos t, b\,\xi\sin t)\,\xi\,\mathrm{d}\xi\,\mathrm{d}t\,. \tag{B.5}$$

Now, we have

$$A = I[1] = ab \int_0^{2\pi} \int_0^{1+f(t)} \xi\,\mathrm{d}\xi\,\mathrm{d}t = \frac{ab}{2}\int_0^{2\pi}\Big(1+f(t)\Big)^2\,\mathrm{d}t\,, \tag{B.6}$$

$$A\sigma_a^2 = I[x^2] = ab \int_0^{2\pi} \int_0^{1+f(t)} a^2\cos^2 t\,\xi^3\,\mathrm{d}\xi\,\mathrm{d}t$$
$$= \frac{a^3 b}{4}\int_0^{2\pi}\cos^2 t\Big(1+f(t)\Big)^4\,\mathrm{d}t\,, \tag{B.7}$$

$$A\sigma_b^2 = I[y^2] = ab \int_0^{2\pi} \int_0^{1+f(t)} b^2\sin^2 t\,\xi^3\,\mathrm{d}\xi\,\mathrm{d}t$$
$$= \frac{ab^3}{4}\int_0^{2\pi}\sin^2 t\Big(1+f(t)\Big)^4\,\mathrm{d}t\,, \tag{B.8}$$

$$\sigma^2 = \sigma_a^2 + \sigma_b^2 = \frac{ab}{4A}\int_0^{2\pi}\Big(a^2\cos^2 t + b^2\sin^2 t\Big)\Big(1+f(t)\Big)^4\,\mathrm{d}t\,. \tag{B.9}$$

If we choose the ellipse to have the same area as the placenta, then we require $A = \pi ab$, and from (B.6) we have

$$\int_0^{2\pi}\Big(1+f(t)\Big)^2\,\mathrm{d}t = 2\pi\,. \tag{B.10}$$

We can then either choose the ellipse to be a circle or to have with same aspect ratio as the placenta.

For the case of a circle, we have $a = b = (A/\pi)^{1/2}$. Then from (B.9) we have

$$\sigma^2 = \frac{A}{4\pi^2}\int_0^{2\pi}\Big(1+f(t)\Big)^4\,\mathrm{d}t\,. \tag{B.11}$$

Alternatively, if we choose the ellipse semi-axes so that the ellipse has aspect ratio $\lambda = \sigma_a/\sigma_b$ as the placenta, we have $a = ((A\lambda)/\pi)^{1/2}$ and $b =$

$(A/(\pi\lambda))^{1/2}$. This implies $a^2\sigma_b^2 = b^2\sigma_a^2$, so from (B.7) and (B.8) we then have

$$\int_0^{2\pi} \left(\cos^2 t - \sin^2 t\right)\left(1 + f(t)\right)^4 \mathrm{d}t = 0 \,. \tag{B.12}$$

Using the identity

$$a^2 \cos^2 t + b^2 \sin^2 t \equiv \tfrac{1}{2}(a^2 - b^2)(\cos^2 t - \sin^2 t) + \tfrac{1}{2}(a^2 + b^2) \tag{B.13}$$

together with (B.9) and (B.12) we find that

$$\sigma^2 = \frac{A}{8\pi^2}\left(\lambda + \lambda^{-1}\right) \int_0^{2\pi} \left(1 + f(t)\right)^4 \mathrm{d}t \,. \tag{B.14}$$

We now take the identity

$$\left(1 + f(t)\right)^4 \equiv 2\left(1 + f(t)\right)^2 - 1 + f(t)^2\left(2 + f(t)\right)^2 \,, \tag{B.15}$$

integrate it between 0 and 2π, and use (B.10) to show that

$$\int_0^{2\pi} \left(1 + f(t)\right)^4 = 2\pi + 2\int_0^{2\pi} f(t)^2\left(1 + \tfrac{1}{2}f(t)\right)^2 \mathrm{d}t \geq 2\pi \,, \tag{B.16}$$

with equality if and only if $f(t) \equiv 0$.

So from (B.11) and (B.14) we have that

$$\sigma^2 \geq \frac{A}{2\pi} \,, \qquad \text{and} \qquad \sigma^2 \geq \frac{A}{4\pi}\left(\lambda + \lambda^{-1}\right) \,, \tag{B.17}$$

with equality in the first case if and only if the placenta is circular, and in the second case if and only if the placenta is elliptical.

This establishes the minimal values for σ^2 quoted in §5.2 and §5.3 which are achieved precisely for circular and elliptical placentas. We also observe that that the second bound in (B.17) is always stricter unless the aspect ratio λ is 1.

Finally, we observe from (B.16) that the expressions (5.12) and (5.20) for β and γ are given in terms of $f(t)$ by

$$\left(\frac{1}{\pi}\int_0^{2\pi} f(t)^2\left(1 + \tfrac{1}{2}f(t)\right)^2 \mathrm{d}t\right)^{1/2} \,. \tag{B.18}$$

Thus if $f(t) = O(\epsilon)$, then β or γ will be $O(\epsilon)$. So for small departures from and ellipse or a circle the measures β and γ behave linearly in the distance of departure. This is the reason for the outer square root in the definitions (5.12) and (5.20).

C R code for calculating the efficiency index

The R code used to compute the efficiency index, as described in §7 is included below:

```r
# Calculates the efficiency of a placenta
# Returns a list:
#   eff = efficiency index
#   D  = map of distances
#   u  = distance per pixel
# System requirements are libtiff for the function read.picture()

Get.efficiency<-function(filename){
 P=read.picture(filename,extensions='tif')
 x=dim(P)[1]
 y=dim(P)[2]
 B=P[,,1]
 B[B>1]=1
 count=sum(B)
 D=P[,,2]
 D[D>1]=1
 c=0
 k=1
 while(c<count){
 write(paste(k,c,count),"")
  i=1;  j=1
    if(D[i,j]==k){
     if(P[i+1,j,1]>1&D[i+1,j]==0){ D[i+1,j]=k+1; c=c+1}
     if(P[i,j+1,1]>1&D[i,j+1]==0){D[i,j+1]=k+1; c=c+1}}
      for(j in 2:(y-1))
    if(D[i,j]==k){
     if(P[i+1,j,1]>1&D[i+1,j]==0){D[i+1,j]=k+1; c=c+1}
     if(P[i,j-1,1]>1&D[i,j-1]==0){D[i,j-1]=k+1; c=c+1}
     if(P[i,j+1,1]>1&D[i,j+1]==0){D[i,j+1]=k+1; c=c+1}
    }
  j=y
    if(D[i,j]==k){
     if(P[i+1,j,1]>1&D[i+1,j]==0){D[i+1,j]=k+1; c=c+1}
     if(P[i,j-1,1]>1&D[i,j-1]==0){D[i,j-1]=k+1; c=c+1}}
  i=x
    if(D[i,j]==k){
    #assign distance to each unassigned point in the placenta
     if(P[i-1,j,1]>1&D[i-1,j]==0){D[i-1,j]=k+1; c=c+1}
     if(P[i,j-1,1]>1&D[i,j-1]==0){D[i,j-1]=k+1; c=c+1}}
  j=1
    if(D[i,j]==k){
```

```r
   #assign distance to each unassigned point in the placenta
    if(P[i-1,j,1]>1&D[i-1,j]==0){D[i-1,j]=k+1; c=c+1}
    if(P[i,j+1,1]>1&D[i,j+1]==0){D[i,j+1]=k+1; c=c+1}}

  for(j in 2:(y-1))
   if(D[i,j]==k){
   #assign distance to each unassigned point in the placenta
    if(P[i-1,j,1]>1&D[i-1,j]==0){D[i-1,j]=k+1; c=c+1}
    if(P[i,j-1,1]>1&D[i,j-1]==0){D[i,j-1]=k+1; c=c+1}
    if(P[i,j+1,1]>1&D[i,j+1]==0){D[i,j+1]=k+1; c=c+1}
   }
  for(i in 2:(x-1)){
  j=1
    #assign distance to each unassigned point in the placenta
    if(P[i-1,j,1]>1&D[i-1,j]==0){D[i-1,j]=k+1; c=c+1}
    if(P[i+1,j,1]>1&D[i+1,j]==0){D[i+1,j]=k+1; c=c+1}
    if(P[i,j+1,1]>1&D[i,j+1]==0){D[i,j+1]=k+1; c=c+1}
  j=y
    #assign distance to each unassigned point in the placenta
    if(P[i-1,j,1]>1&D[i-1,j]==0){D[i-1,j]=k+1; c=c+1}
    if(P[i+1,j,1]>1&D[i+1,j]==0){D[i+1,j]=k+1; c=c+1}
    if(P[i,j-1,1]>1&D[i,j-1]==0){D[i,j-1]=k+1; c=c+1}
   for(j in 2:(y-1)){
    if(D[i,j]==k){
    #assign distance to each unassigned point in the placenta
    if(P[i-1,j,1]>1&D[i-1,j]==0){D[i-1,j]=k+1; c=c+1}
    if(P[i+1,j,1]>1&D[i+1,j]==0){D[i+1,j]=k+1; c=c+1}
    if(P[i,j-1,1]>1&D[i,j-1]==0){D[i,j-1]=k+1; c=c+1}
    if(P[i,j+1,1]>1&D[i,j+1]==0){D[i,j+1]=k+1; c=c+1}
    }
   }
  }
k=k+1
 }

cc=0;
#calculate the number of points to make 5 cm
for(c in 1:x)cc=ifelse(sum(P[c,,3])>0,cc+1,cc)
#calculate the length of a unit
u=5/cc
d=1/(u*(D-1)+1)
d[d>1]=0
eff=(u^2)*sum(d)
list(eff=eff,D=D,u=u)
}
```

Part VI
References

References

ABRAMOWITZ, M. & STEGUN, I. A. (ed.) 1964 *Handbook of Mathematical Functions with Formulas, Graphs, and Mathematical Tables. National Bureau of Standards Applied Mathematics Series* 55. U.S. Government Printing Office, Washington, DC.

BISWAS, S. & GHOSH, S. K. 2008 Gross morphological changes of placentas associated with intrauterine growth restriction of fetuses: A case control study. *Early Hum. Dev.* **84** (6), 357–362.

BONFIGLIO, A., LEUNGCHAVAPHONGSE, K., REPETTO, R. & SIGGERS, J. H. 2010 Mathematical modeling of the circulation in the liver lobule. *ASME J Biomech Eng* To appear.

BURTON, G. J., WATSON, A. L., HEMPSTOCK, J., SKEPPER, J. N. & JAUNIAUX, E. 2002 Uterine glands provide histiotrophic nutrition for the human foetus during the first trimester of pregnancy. *J. Clin. Endocrin. Metab.* **87**, 2954–2959.

CHERNYAVSKY, I. L., JENSEN, O. E. & LEACH, L. 2010 A mathematical model of the intervillous blood flow in the human placentone. *Placenta* To appear.

FRANKE, V., PARKER, K. H., WEE, L. Y., FISK, N. M. & J., S. S. 2003 Time domain computational modelling of 1D arterial networks in monochorionic placentas. *ESAIM: Mathematical Modelling and Numerical Analysis* **37** (4), 557–580.

GEVA, E., GINZINGER, D. G., ZALOUDEK, C. J., MOORE, D. H., BYRNE, A. & JAFFE, R. B. 2002 Human placental vascular development: Vasculogenic and angiogenic (branching and nonbranching) transformation

is regulated by vascular endothelial growth factor-A, angiopoietin-1, and angiopoietin-2. *J. Clin. Endocrin. Metab.* **87**, 4213–4224.

GORDON, C., WEBB, D. L. & WOLPERT, S. 1992 One cannot hear the shape of a drum. *Bulletin of the American Mathematical Society* **27**, 134—138.

HEAZELL, A. & FRØEN, J. 2008 Methods of fetal movement counting and the detection of fetal compromise. *J. Obstet. Gynaecol.* **28** (2), 147–154.

KAC, M. 1966 Can one hear the shape of a drum? *The American Mathematical Monthly* **73** (4, part 2), 1–23.

R DEVELOPMENT CORE TEAM 2009 *R: A Language and Environment for Statistical Computing*. R Foundation for Statistical Computing, Vienna, Austria.

ROCKAFELLAR, R. T. 1970 *Convex Analysis*, *Princeton Mathematical Series*, vol. 28. Princeton University Press, Princeton, NJ.

ROCKAFELLAR, R. T. & WETS, R. J.-B. 1998 *Variational Analysis*, *Grundlehren der matematischen Wissenschaften*, vol. 317. Springer-Verlag, Berlin Heidelberg.

SALAFIA, C. & YAMPOLSKY, M. 2009 Metabolic scaling law for fetus and placenta. *Placenta* **30** (5), 468–471.

SMITH, C. R. 1968 A characterization of star-shaped sets. *The American Mathematical Monthly* **75** (4), 386.

STEWART, I. 2009 Placentation. University of Aberdeen Lecture notes. `http://www.abdn.ac.uk/sms/ugradteaching/DB3502/DB3502_1822009_9.ppt`.

WARRANDER, L. & HEAZELL, A. 2010 Identifying placental dysfunction in women with reduced fetal movements can be used to predict patients at increased risk of pregnancy complications. *Med. Hypotheses* In press.

WIKIPEDIA CONTRIBUTORS 2010 Chirion. In *Wikipedia*. Wikimedia Foundation. `http://en.wikipedia.org.wiki/Chirion`.

YAMPOLSKY, M., SALAFIA, C. M., SHLAKHTER, O., HAAS, D., EUCKER, B. & THORP, J. 2008 Modeling the variability of shapes of a human placenta. *Placenta* **29** (9), 790–7.

Yampolsky, M., Salafiab, C. M., Shlakhterd, O., Haase, D., Euckerf, B. & Thorpf, J. 2009 Centrality of the umbilical cord insertion in a human placenta influences the placental efficiency. *Placenta* **30** (12), 1058–1064.